Univerzita Karlova v Praze

Matematicko-fyzikální fakulta

BAKALÁŘSKÁ PRÁCE

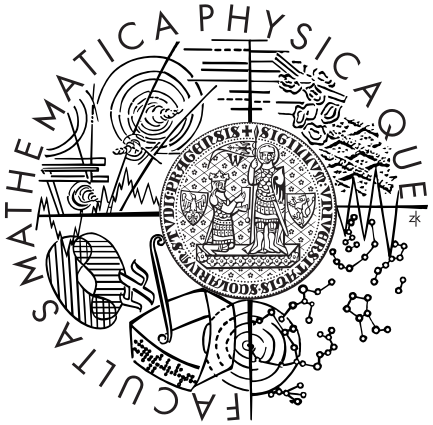

Michal Habera

Numerické simulace ferrotekutin

Matematický ústav UK

Vedoucí bakalářské práce: RNDr. Ing. Jaroslav Hron, Ph.D.

Studijní program: Fyzika

Studijní obor: Obecná fyzika

Praha 2015

Charles University in Prague
Faculty of Mathematics and Physics

BACHELOR THESIS

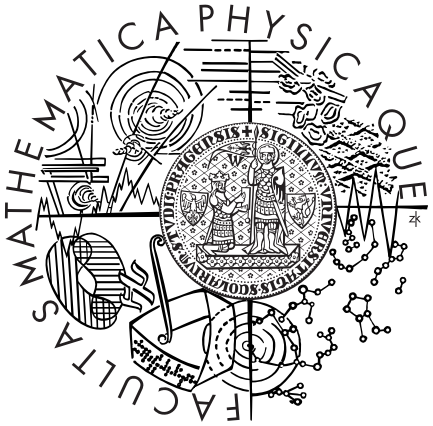

Michal Habera

Numerical simulation of ferrofluids

Mathematical Institute of Charles University

Supervisor of the bachelor thesis: RNDr. Ing. Jaroslav Hron, Ph.D.

Study programme: Physics

Specialization: General Physics

Prague 2015

I declare that I carried out this bachelor thesis independently, and only with the cited sources, literature and other professional sources.

I understand that my work relates to the rights and obligations under the Act No. 121/2000 Coll., the Copyright Act, as amended, in particular the fact that the Charles University in Prague has the right to conclude a license agreement on the use of this work as a school work pursuant to Section 60 paragraph 1 of the Copyright Act.

In ..... date ..... signature of the author

I owe a great many thanks to the supervisor, RNDr. Ing. Jaroslav Hron, Ph.D., for many hours of fruitful discussions and reflections.

I am also immensely grateful to my family and friends for their support, mental and financial.

My parents, Zuzana and Ján, receive my deepest gratitude and love for their dedication and the years of support during my studies.

Last but not least, many thanks go to my beloved girlfriend Zuzana, for all her love and encouragement.

Název práce: Numerické simulace ferrotekutin

Autor: Michal Habera

Katedra: Matematický ústav UK

Vedoucí bakalářské práce: RNDr. Ing. Jaroslav Hron Ph.D., Matematický ústav UK

Abstrakt: Tenzor napätia ferrokvapaliny vystavenej vonkajšiemu magnetickému poľu podlieha navyše magnetickým členom. Pre lineárne magnetizovateľné médium tieto členy vedú na magnetickú silu pôsobiacu na hranici ferrokvapaliny. Táto sila mení charakteristiky množstva javov s voľným povrchom ferrokvapaliny. Cieľom tejto práce je implementovať túto silu do nestlačiteľných Navier-Stokesových rovníc a navrhnúť numerickú metódu na ich riešenie. Rozhranie ferrokvapaliny je sledované s pomocou level-set metódy a dodatočný krok reinicializácie zaisťuje zachovanie objemu. Nestlačieľné Navier-Stokesové rovnice sú formulované pre rýchlostné polia s nulovou divergenciou pričom diskrétne sily na rozhraní sú ošetrené modelom spojitých povrchových síl. Rýchlostno-tlakové previazanie je dané projekčnou metódou. Z dôvodu kvantitatívnej predpovede vplyvu magnetickej sily sú pre každý časový krok riešené Maxwellove rovnice magnetostatiky. Metóda konečných prvkov je použitá pre priestorovú diskretizáciu. Na záver práce sú kvalitatívne porovnané známe experimenty s nasimulovaným rovnovážnym tvarom ferrokvapalinovej kvapky a javom odkvapávania.

Klíčová slova: ferrohydrodynamika, ferrokvapalina, level-set, odkvapávanie

Title: Numerical simulation of ferrofluids

Author: Michal Habera

Department: Mathematical Institute of Charles University

Supervisor: RNDr. Ing. Jaroslav Hron, Ph.D., Mathematical Institute of Charles University

Abstract: The stress tensor of a ferrofluid exposed to an external magnetic field is subject to an additional magnetic terms. For a linearly magnetizable medium, such terms results in an interfacial magnetic force acting on the ferrofluid boundaries. This force changes the characteristics of many free-surface ferrofluid phenomena. The aim of this work is to implement this force into Navier-Stokes equations and propose a numerical method to solve them. The interface of ferrofluid is tracked with the use of level-set method and additional reinitialization step assures conservation of its volume. Incompressible Navier-Stokes equations are formulated for divergence free velocity fields while discrete interfacial forces are treated with continuous surface force model. Velocity-pressure coupling is given by projection method. To predict the magnetic force effect quantitatively, Maxwell's equations for magnetostatics are solved in each time step. Finite element method is utilized for the spatial discretization. At the end of the work, equilibrium droplet shape and dripping phenomenon are qualitatively compared to known experimental results.

Keywords: ferrohydrodynamics, ferrofluid, level-set, dripping

Contents

Introduction **3**

1 Ferrofluids **4**
1.1 Introduction 4
1.2 Ferrohydrodynamics 5
1.2.1 Magnetostatics for non-conducting materials 5
1.2.2 Magnetic stress tensor 6
1.2.3 Classification of "pressures" in ferrofluid 7
1.2.4 Reduced magnetic force density form 8
1.2.5 Equation of motion for a ferrofluid 8

2 The Finite element method **9**
2.1 Problem definition 9
2.2 Weak solution and basis, variational formulation 9
2.3 Principles and algorithm 10
2.4 Finite element spaces 11
2.5 Automated FEM, FEniCS project 11

3 The Level-Set method **12**
3.1 Mathematical formulation 12
3.2 Level-set advection 13
3.3 FEM for the level-set advection 15
3.3.1 Time discretization 16
3.4 FEM for the level-set reinitialization 16
3.4.1 Time discretization 17
3.5 The advection step summary 17

4 The ferrofluid Navier-Stokes equations **18**
4.1 The equations and continuous surface force approach 18
4.1.1 The continuous surface tension force 19
4.1.2 The continuous magnetic force 20
4.2 Dimensionless form 20
4.3 Numerical solution and projection methods 21
4.3.1 Finite element formulation 22

5 Equilibrium ferrofluid droplet shape **23**
5.1 Problem definition 23
5.2 FEM for magnetostatics 24
5.2.1 Magnetic field of ferrofluid droplet 25
5.2.2 Evolution to the equilibrium shape 26

6 Ferrofluid dripping phenomenon **30**
6.1 Problem definition 30
6.2 Qualitative comparison 31

Conclusion **35**

Bibliography **37**

List of Tables **40**

List of Abbreviations **41**

Introduction

Free surface fluid flows and processes involved in a fluid behavior fascinated scientists since the very beginning of the scientific history. Problems as a breakup of a liquid jet, droplet formation and merging, rising bubbles etc. still lacks deeper understanding because of a complex and nonlinear equations governing such phenomena. In addition, they play a role in many industrial processes: *fuel injection, fibre spinning, ink-jet printing, etc.* [2]

The equations for the motion of a fluid formulated in the 19th century came to relevance as computers started to provide number of numerical methods for finding their approximate solutions. However, majority of the methods are well suited for problems involving one-phase flows or fluid-wall interactions. Multiphase flows, fluid-fluid interactions, surface forces and similar issues still remain debated and incomplete.

Imagine some usual situation, where a water droplet hanging on a tap is being pulled down by the gravity. From a physical point of view, the behavior and evolution is well described. *Navier-Stokes* equations govern the fluid motion in each phase, water and air separately, while interfacial surface force is balanced with the gravitational, volume force.

All these phenomena become even more attractive in terms of *ferrohydrodynamics*. Ferrofluid reacts to a magnetic field and changes its shape due to an additional magnetic force. This entirely changes dynamics of the droplet formation process and it will be the object for our studies.

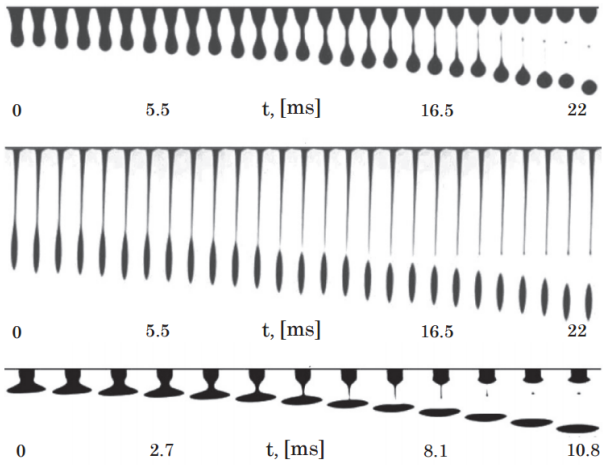

Figure 1: High-speed image sequence of ferrofluid droplet dripping out of a container. Influence of a magnetic field parallel(middle) and perpendicular(bottom) to the direction of the flow is clearly visible. Taken from [1].

In the first part of the thesis a brief summary of the physical and mathematical model and numerical methods are given. Interface is represented with the *level-set* function, while the conservation of its volume is assured with the reinitialization step. Navier-Stokes equations are solved using the *projection methods* and spatially approximated in sense of weak derivates and *finite element method*.

1. Ferrofluids

1.1 Introduction

A **ferrofluid** is a colloidal suspension composed of small (3-15 nm) solid, single-domain, magnetic particles coated with a molecular layer of a dispersant and suspended in a liquid carrier(Fig. 1.1). Thermal agitation keeps the particles suspended(under sufficient stability conditions) because of the Brownian motion and the coatings prevents the particles from sticking to each other.

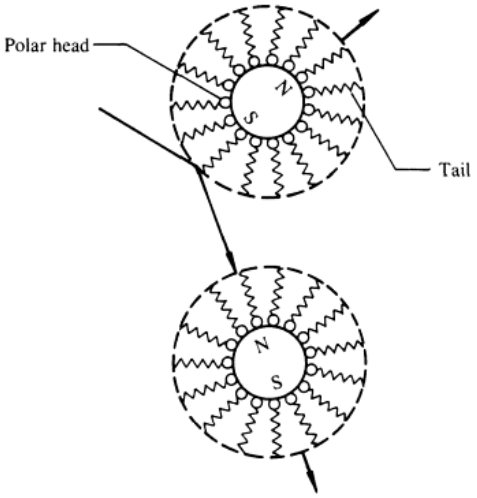

Figure 1.1: Coated magnetic particles in ferrofluid. Taken from [3].

The magnetic ferrofluids of the type in general use today are an outgrowth of discoveries made in the early 1960s.

Because the colloidial ferrofluid is not found in the nature, it must be synthetized. Methods called *size reduction* and *chemical precipitation* are used. Details of both methods can be found in [3].

Very important property of ferrofluid is its stability. It ensures the investigator of well-defined material for scientific studies and also fluid applications. We mean

- *stability in a magnetic field gradient*,
- *stability against settling in a gravitational field*,
- *stability against magnetic agglomeration* and
- *neccesity to guard against the van der Waals attractive force.*

To derive the physicochemical stability dimensionless analysis introduces various energy terms:

- *thermal energy* kT,
- *magnetic energy* $\mu_0 MHV$ and

- *gravitational energy* $\Delta\rho VgL$,

where k is Boltzmann's constant, T the absolute temperature in degrees Kelvin, μ_0 is the permeability of free space, V volume of a sperical particle, L the elevation in gravitational field, $\Delta\rho$ difference in fluid carrier and ferromagnetic particles densities and M, H magnetization and magnetic field intensity.

Such stability analysis leads to inequalities for the particle diameter, for instance, for the magnetite(Fe_3O_4) particles at the room temperature stability against magnetic agglomeration requires diameter $d \leq 7.8$ nm [3].

1.2 Ferrohydrodynamics

The term **ferrohydrodynamics** (FHD) was first introduced by **Ronald E. Rosensweig**. Development of FHD in early to mid- 1960s was motivated by engineering task of converting heat to work with no mechanical parts.

"*Ferrohydrodynamics is an interdisciplinary topic having inherent interest of a physical and mathematical nature with applications in tribology, separations science, instrumentation, information display, printing, medicine, and other areas*" R.E.Rosensweig.

In the begining of this chapter we would like to emphasize the differences between various studies of fluid–field interactions:

1. *electrohydrodynamics* (EHD) deals with the influence of the electric field on a fluid motion,

2. *magnetohydrodynamics* (MHD) is the study of the interaction between magnetic field and fluid conductors of electricity,

3. *ferrohydrodynamics* (FHD) deals with the mechanics of fluid motion influenced by forces of magnetic polarization.

This work is mainly concerned with ferrohydrodynamics, because ferrofluids are non–conducting therefore there is zero Lorentz force acting as body force(in contrast with MHD). The body force in FHD is due to *polarization force* which requires material magnetization in presence of magnetic field gradients or discontinuities.

1.2.1 Magnetostatics for non-conducting materials

Here we give very brief summary of physical laws and relations for magnetic field in matter. More details could be found in [4, 5].

Magnetostatics is related to the phenomena, where the electric field **E**, electric displacement field **D** and currents **J** are zero. Such assumption is not fully justified, because the existence of magnetic field is a result of currents and currents are present when charges are moving. Therefore, magnetostatics is only an approximation.

The existence of magnetic field on *macroscopic level* without currents is based on the *quantum theory*. It is mainly the spin magnetic moments that contribute to

the molecular fields. Maxwell's equations with the previous assumptions reduce to the set

$$\nabla \cdot \mathbf{B} = 0, \tag{1.1}$$

and

$$\nabla \times \mathbf{H} = 0, \tag{1.2}$$

where $\mathbf{B}$ is the *magnetic induction* and $\mathbf{H}$ is the *magnetic field intensity*.

In addition to the equations (1.1, 1.2) so called *constitutive relations* between $\mathbf{H}$ and $\mathbf{B}$ must be provided, formally

$$\mathbf{H} = \mathbf{H}(\mathbf{B}). \tag{1.3}$$

The material is said to be *linear* iff in an index notation

$$H_i = \sum_j (\mu^{-1})_{ij} B_j,$$

where $(\mu^{-1})_{ij}$ is the *inverse magnetic permeability tensor*. In the simplest case, the linear response is *isotropic* and the $(\mu^{-1})_{ij}$ tensor is diagonal with all diagonal elements equal. Thus, for the linear, isotropic media

$$\mathbf{H} = \mu^{-1}\mathbf{B}, \ \mathbf{B} = \mu\mathbf{H}, \tag{1.4}$$

with μ the *absolute material permeability*.

At the macroscopic level, it is reasonable to define the *magnetization* or macroscopically averaged dipole moment of the medium $\mathbf{M}$ as

$$\mathbf{B} = \mu_0(\mathbf{H} + \mathbf{M}). \tag{1.5}$$

where $\mu_0 = 4\pi 10^{-7}\ \mathrm{H\,m^{-1}}$ is the permeability of free space. Expressing $\mathbf{M}$ explicitly and from the equation (1.4) simply follows that

$$\mathbf{M} = \chi\mathbf{H},$$

with $\chi := \left(\frac{\mu}{\mu_0} - 1\right)$ the *magnetic susceptibility* of the medium.

In this thesis, all of the physical quantities are defined and represented in the *International System of Units*, so magnetic induction $\mathbf{B}$ is measured in *teslas* T and magnetic field $\mathbf{H}$ is measured in amperes per metre, $\mathrm{A\,m^{-1}}$.

1.2.2 Magnetic stress tensor

As we have mentioned above, understanding the differences between several fluid–field interactions play important role in a development of a physical model for the flow of a ferrofluid.

The only body force acting from the outside in hydrodynamics is gravitational. In electrohydrodynamics electrically charged particles are affected with electrical forces while in magnetohydrodynamics conductive fluid is subject to the Lorentz body force.

The derivation of the *magnetic stress tensor* with respect to the thermodynamic background and conservation of energy leads to [3]

$$\mathbf{T}'_m = -\left[p(\rho,T) + \int_0^H \mu_0 \left(\frac{\partial(\nu M)}{\partial \nu}\right)_{\tilde{H},T} \mathrm{d}\tilde{H} + \frac{1}{2}\mu_0 H^2\right]\mathbf{I} + \mathbf{B}\otimes\mathbf{H}, \tag{1.6}$$

where notation from [3] is adopted so $\mathbf{B}\otimes\mathbf{H} = B_i H_j$ represents dyadic product, p is thermodynamic pressure, ρ the density, T thermodynamic temperature, H, M associated magnitude of the magentic field and magnetization respectively ($H := \|\mathbf{H}\|$, $M := \|\mathbf{M}\|$), $\nu = \rho^{-1}$ the specific volume, $\mathbf{I}$ the identity tensor and $\mathbf{B}$ magnetic induction. The notation

$$\left(\frac{\partial(\nu M)}{\partial \nu}\right)_{\tilde{H},T}$$

means, that derivative is evaluated at constant $\tilde{H}$ and T, because M is also a function of a magnetic field.

Note, that the *tensor is symmetric*, because $\mathbf{B}\otimes\mathbf{H} = \mathbf{H}\otimes\mathbf{B}$ follows from (1.4) and $\mathbf{I} = \mathbf{I}^{\mathrm{T}}$. This result holds also for nonlinear effects, i.e. nonlinear magnetization $\mathbf{M}$ of the ferrofluid.

1.2.3 Classification of "pressures" in ferrofluid

In the expression for the magnetic stress tensor, thermodynamic pressure $p = p(\rho,T)$ appeared naturally as a result of the derivation. In order to emphasize the magnetic aspect of the result we define a new tensor $\mathbf{T}_m$ such that

$$\mathbf{T}_m := \mathbf{T}'_m + p(\rho,T)\mathbf{I}$$

so we separated thermodynamic pressure present also in non–polar fluid. The new tensor is

$$\mathbf{T}_m = -\left[\int_0^H \mu_0 \left(\frac{\partial(\nu M)}{\partial \nu}\right)_{\tilde{H},T} \mathrm{d}\tilde{H} + \frac{1}{2}\mu_0 H^2\right]\mathbf{I} + \mathbf{B}\otimes\mathbf{H}, \tag{1.7}$$

and the *magnetic force per unit volume* corresponding to a magnetic stress tensor $\mathbf{T}_m$ is

$$\mathbf{f}_m = \nabla\cdot\mathbf{T}_m. \tag{1.8}$$

There is an arbitrariness in grouping of magnetic terms in (1.7) that has led to some confusion in the literature. Here, we follow the classification introduced in [3].

Applying the partial derivative in the term $\frac{\partial(\nu M)}{\partial \nu}$ and in the sense of the equation $\mathbf{f} = \nabla p$, some pressure–like terms in (1.7) are identified.

The **magnetostrictive pressure**

$$p_s := \mu_0 \int_0^H \nu \left(\frac{\partial M}{\partial \nu}\right)_{H,T} \mathrm{d}H, \tag{1.9}$$

and the **fluid-magnetic pressure**

$$p_m := \mu_0 \int_0^H M \mathrm{d}H. \tag{1.10}$$

Applying definitions (1.9, 1.10) and relation (1.4), expression for the magnetic stress tensor yields

$$\mathbf{T}_m = -(p_s + p_m + \frac{1}{2}\mu_0 H^2)\mathbf{I} + \mu \mathbf{H} \otimes \mathbf{H}. \tag{1.11}$$

1.2.4 Reduced magnetic force density form

It could be shown due to *Korteweg and Helmholtz* that for *linearly magnetizable media* magnetic force density reduces to

$$\mathbf{f}_m = \nabla \left[\frac{H^2}{2} \rho \left(\frac{\partial \mu}{\partial \rho} \right)_T \right] - \frac{H^2}{2} \nabla \mu.$$

For media with absolute permeability constant within each phase separately, $\frac{\partial \mu}{\partial \rho} \equiv 0$ almost everywhere, therefore the magnetic force density is

$$\mathbf{f}_m = -\frac{H^2}{2} \nabla \mu. \tag{1.12}$$

This force vanishes everywhere except for the phase interfaces, where non–zero jump in the absolute permeability μ is present.

Such analysis is crucial in the experiments, where constant permeability is assumed everywhere except for the phase interfaces. The magnetic force acts on the boundaries with the effect similar to the surface tension force.

1.2.5 Equation of motion for a ferrofluid

Very important part of ferrohydrodynamics is devoted to the formulation and study of equation of motion for a ferrofluid. A momentum equation was first proposed by Neuringer and Rosensweig (1964) [6]. In order to satisfy the continuum mechanics assumptions, it is assumed, that the dynamic equilibrium holds for an "infinitesimal element", which is large enough to contain a large number of colloidial magnetic particles comparing to the dimensions of the flow field.

The Newton's law for such "infinitesimal" element yields

$$\rho \left(\partial_t \mathbf{u} + (\mathbf{u} \cdot \nabla) \mathbf{u} \right) = \underbrace{f_p}_{\text{Pressure force}} + \underbrace{f_v}_{\text{Viscous force}} + \underbrace{f_g}_{\text{Gravity force}} + \underbrace{f_m}_{\text{Magnetic force}} + \underbrace{f_s}_{\text{Surface tension force}} \tag{1.13}$$

The equation (1.13) with the magnetic force density expression (1.12) simply unfolds the effect of a magnetic field on an incompressible linearly magnetizable ferrofluid, but more formal and rigorous problem definition with appropriate simplifications is given in the form of the *Navier-Stokes equations* in the chapter 4.

2. The Finite element method

In the following sections we give a very brief introduction into the finite element method. We also refer more advanced reader who seeks more detail to [7] and for mathematical insight to [8].

2.1 Problem definition

We are interested in a solution of a partial differential equations of the type

$$\mathcal{L}(u(\mathbf{x})) = f(\mathbf{x}),\ \forall \mathbf{x} \in \Omega \tag{2.1}$$

on a given domain Ω, where $\mathcal{L}$ is a linear differential operator, $u = u(x_1, \ldots, x_n) =: u(\mathbf{x})$ and $f = f(x_1, \ldots, x_n) =: f(\mathbf{x})$ is some known right hand side.

It is necessary to impose boundary conditions on the boundary $\partial\Omega$ of the domain. These conditions are usually of type *Dirichlet*, so that

$$u = b_D(\mathbf{x}),\ \forall \mathbf{x} \in \partial\Omega$$

where b_D is a prescribed function. Another type of the boundary condition is so called *Neumann*, where

$$\nabla u \cdot \mathbf{n}(\mathbf{x}) = b_N(\mathbf{x}),\ \forall \mathbf{x} \in \partial\Omega$$

where $\mathbf{n}$ is unit normal to the boundary.

2.2 Weak solution and basis, variational formulation

Yet, we didn't define function spaces for the functions in the problems like (2.1). This is very important part and plays significant role in the finite element method.

Let us find such solutions to our problem, that the desired function u is in some space $\mathcal{S}$. It is reasonable, to suppose, that the space is rich enough, to contain all the solutions.

We define the inner product of two functions on Ω

$$(f(\mathbf{x}), g(\mathbf{x})) := \int_\Omega fg \ \mathrm{d}\mathbf{x}$$

and norm induced by the inner product

$$||f|| := \sqrt{(f, f)}.$$

We say, that u is a **weak solution** to the problem (2.1), if

$$(\mathcal{L}(u) - f, s) = 0,\ \forall s \in \mathcal{S}. \tag{2.2}$$

Function $s = s(\mathbf{x})$ is often refered as a *test function*. It is clear, that the space $\mathcal{S}$ is not of finite dimension. This is a very restrictive condition. One might try

to find an approximation of a solution, $\tilde{u}(\mathbf{x})$ in a finite dimensional subspace, say $\mathcal{S}_n$, where $n \in \mathbb{N}_1$ is a dimension of this space. Let then $\{s_i(\mathbf{x})\}, i = 1, \ldots, n$ be the *basis* of this space, so each function from our subspace $\mathcal{S}_n$ can be expressed as a linear combination of the basis functions

$$\tilde{u} = c_i s_i,$$

where summation convention is used.

The equation (2.2) could be written in terms of the variational formulation. If we let

$$L(s) := \int_\Omega s f \mathrm{d}\mathbf{x}$$

and

$$a(\tilde{u}, s) := \int_\Omega \mathcal{L}(\tilde{u}) s \mathrm{d}\mathbf{x},$$

the problem (2.1) becomes an equality of the (uni)linear and bilinear form. The linearity of the forms is clear from the linearity of the Lebesgue integral.

2.3 Principles and algorithm

We are thus interested in seeking a solutions of (2.2). This can be rewritten taking $s_j(\mathbf{x})$ as the test function

$$(\mathcal{L}(\tilde{u}), s_j) = (f, s_j)$$

and decomposing approximate solution into the finite basis

$$(\mathcal{L}(c_i s_i), s_j) = (f, s_j),$$
$$c_i(\mathcal{L}(s_i), s_j) = (f, s_j).$$

We let

$$\mathbf{A} := A_{ij} := \{(\mathcal{L}(s_i), s_j)\},$$
$$\mathbf{b} := \{(f, s_j)\}$$

and

$$\mathbf{c} := \{c_i\}$$

set of the coefficients we are interested in. This is clearly a system of the equations known from linear algebra, $\mathbf{Ac} = \mathbf{b}$.

We have derived the set of the equations that solves our problem in sense of a weak solution given by the condition (GALERKIN).

Let suppose, for the sake of simplicity, that $\Omega \subset \mathbb{R}^2$. Integral over Ω induced by the inner product is decomposed into the sum of integrals over subdomains of Ω. In sense of FEM, such decomposition is done into triangles, e.g. a **triangulation** in $\mathbb{R}^2$ into M cells.

We write

$$\Omega =: \bigcup_{k=1}^{M} T_k,$$

so the matrix elements become

$$A_{ij} = \int_\Omega \mathcal{L}(s_i) s_j \mathrm{d}\mathbf{x} = \sum_{k=1}^{M} \int_{T_k} \mathcal{L}(s_i) s_j \mathrm{d}\mathbf{x}.$$

2.4 Finite element spaces

The basis functions s_i were not yet specified.

Because the system $\mathbf{Ac} = \mathbf{b}$ is solved, we would like them to vanish almost everywhere, i.e. to have non-zero value only on some element(triangle) with its neighbours. This implies, that the inner product $A_{ij} = (\mathcal{L}(s_i), s_j)$ forms a sparse matrix.

In the following, we refer to the **type** of the element. A type is simply a class of basis functions. Most common choice of this class is so called *Lagrange* polynomials.

The **order** is roughly the order of the interpolation polynomial.

The **shape** of the finite element is the geometry that defines the decomposition of Ω.

For instance the finite element of type Lagrange, third order and triangular shape means continuous functions on the domain Ω such that on each triangle T_k of the triangulation of Ω the functions are cubic polynomials, i.e. continuous and piecewise cubic polynomials.

We introduce the notation from [9]. Summary of finite element spaces is in table (2.1).

$\mathcal{W}_c^1$	linear	continous
$\mathcal{W}_c^2$	quadratic	continous
$\mathcal{W}_{vc}^1$	linear	vector, continous, $\mathcal{W}_c^1 \times \mathcal{W}_c^1$

Table 2.1: Finite element spaces used in this thesis.

2.5 Automated FEM, FEniCS project

Assembly of linear algebra system and process of its solving is the heart of the finite element method. However, matrix systems become bulky and a quest for the solution could be time demanding. On the other hand, matrices are sparse and in many cases iterative Krylov solvers could decrease computational time.

Together with a problem definition, construction of basis function and, boundary conditions specification finite element method becomes ample tool and automatization of these routines is neccessary.

In this thesis, all of these routines are implemented with the ease of *FEniCS Project*.

"*FEniCS has an extensive list of features for automated, efficient solution of differential equations, including automated solution of variational problems, automated error control and adaptivity, a comprehensive library of finite elements, high performance linear algebra and many more.*" FEniCS Project.

For more detail on FEniCS, we refer to [10].

3. The Level-Set method

Our main goal is the simulation of two-phase flow. It is therefore evident, that a method for *interface tracking* must be implemented.

The **level-set method** (LSM) is simple and straightforward mathematical construction that represents the interface as a cross section of some implicit hypersurface. Recent studies [11] improved the level-set method and reduced several drawbacks of original formulation. The level-set method presented in our work conserves volume of fluid. This improvement is important, especially if we would like to analyse the volume of droplets, jets, etc.

Several other methods for the interface tracking are common, namely *VOF* (volume-of-fluid), *VOSET* (a coupled volume-of-fluid and level-set), *Particle Level-Set*, *Phase-field* etc. [12].

One of the most agreedable benefit of the level-set method is absence of the internal boundary conditions, boundary conditions between multiple phases at their interface. In fact, since interface is captured implicitly, from the mathematical point of view there is no internal boundary. Phase transition occurs smoothly, so as other physical quantities.

Another very important attribute is its simplicity. Even for very complex and topologically bont domains and interfaces. An ordinary problem - multiple circular bubbles merging together would formally require arduous parametrizations dramatically changing as time evolves. In addition, if two bubbles merge, parametrization changes in its very profoundness. Level-set method meets these topological issues in smooth and effective way.

3.1 Mathematical formulation

Let say, domain $\Omega \subset \mathbb{R}^n$. We choose a domain $\Omega_1 \subset \Omega$ that represents one fluid phase. Let then $\Omega_2 = \Omega \backslash \overline{\Omega_1}$. We define the interface between two phases as the finite intersection of all closed sub-domains,

$$\Gamma = \{\mathbf{x} : \mathbf{x} \in \cap \overline{\Omega}_i\}.$$

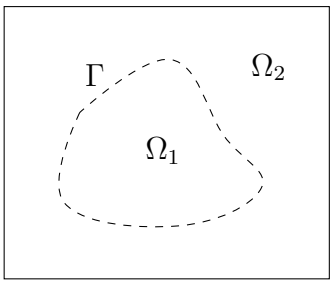

Figure 3.1: Decomposition of domain Ω into subdomain Ω_1 and Ω_2 for each fluid phase. The interface Γ is the object for our studies.

General idea of LSM is to introduce the **level-set function**[1] $\phi(\mathbf{x}) : \Omega \mapsto \mathbb{R}$,

[1] We refer to the level-set function often simply as level-set, e.g. to define the level-set, to transport the level-set, etc.

$K \in \mathbb{R}$ constant, so that the interface is

$$\Gamma = \{\mathbf{x} : \phi(\mathbf{x}) = K\}.$$

The name level-set is derived from the fact, that surface is represented with the K-level plane cross section of some hypersurface.

Standard level-set function, often refered as the **distance level-set function** is defined such that

$$|\phi_d(\mathbf{x})| := \min_{\tilde{\mathbf{x}} \in \Gamma} |\mathbf{x} - \tilde{\mathbf{x}}|, \ K := 0,$$

with $\phi(\mathbf{x}) > 0$ on the one side of the interface and $\phi(\mathbf{x}) < 0$ on the other. The specific property of this function is, that value at each point $\mathbf{x} \in \Omega$ is the minimal distance from $\mathbf{x}$ to the interface Γ.

In this thesis, an interface is tracked with the **characteristic level-set function**. It is an adjustment introduced in [11]. The specific property for this function is, that it is being smoothed characteristic function of one fluid phase. Characteristic function could be mathematically reformulated as $\zeta(\mathbf{x}) \equiv 1 \Leftrightarrow (\mathbf{x} \in \Omega_1)$ and $\zeta(\mathbf{x}) \equiv 0 \Leftrightarrow (\mathbf{x} \in \Omega_2)$.

There are numerous ways of regularization of the characteristic function. We use

$$\phi_c(\mathbf{x}) := \frac{1}{1 + e^{(\phi_d(\mathbf{x})/\varepsilon)}}, \ K := 0.5, \tag{3.1}$$

with $\varepsilon \in \mathbb{R}$ as the "thickness" of the interface. Indeed, on the interface $\phi_d = 0 \Rightarrow \phi_c = 0.5$.

For instance, to constitute a 2D bubble centered in $\mathbf{x}_c \in \Omega_1$ with the radius $r \in \mathbb{R}$, we take the distance level-set $\phi_d(\mathbf{x}) := \|\mathbf{x} - \mathbf{x}_c\| - r$ and substitute into (3.1). Wireframe plot of this level-set is in Fig. (3.2).

Level-set defined analytically as in (3.1) is essential only in process called *initialization*. Later on, level-set is advected and reinitialized as described below and it amends its shape. In contrast, the "thickness" parameter ε plays important role also in reinitialization process.

3.2 Level-set advection

Let assume velocity field $\mathbf{u}(\mathbf{x}, t) : \Omega \times \mathbb{R}^+ \mapsto \mathbb{R}^n$ is given. Let also assume, that the interface is given as described above, represented with the level-set $\phi(\mathbf{x}, t)$. In order to transport the level-set, i.e. to transport the interface, so called *transport equation* must be solved,

$$\partial_t \phi + \mathbf{u} \cdot \nabla \phi = 0, \ \mathbf{x} \in \Omega. \tag{3.2}$$

Explicit solution for this equation could be found. This solution transports the initial level set $\phi(\mathbf{x}, 0)$ with the velocity field $\mathbf{u}$ without change in its profile. Unfortunately, it is not possible to solve this equation numerically and preserve the profile as expected. Depending on the time discretization scheme, several drawbacks are significant (dissipation, dispersion, etc.)[13].

These effects are not desired, because the level-set property(the distance function, the characteristic function) is not retained. To overcome this drawback, it

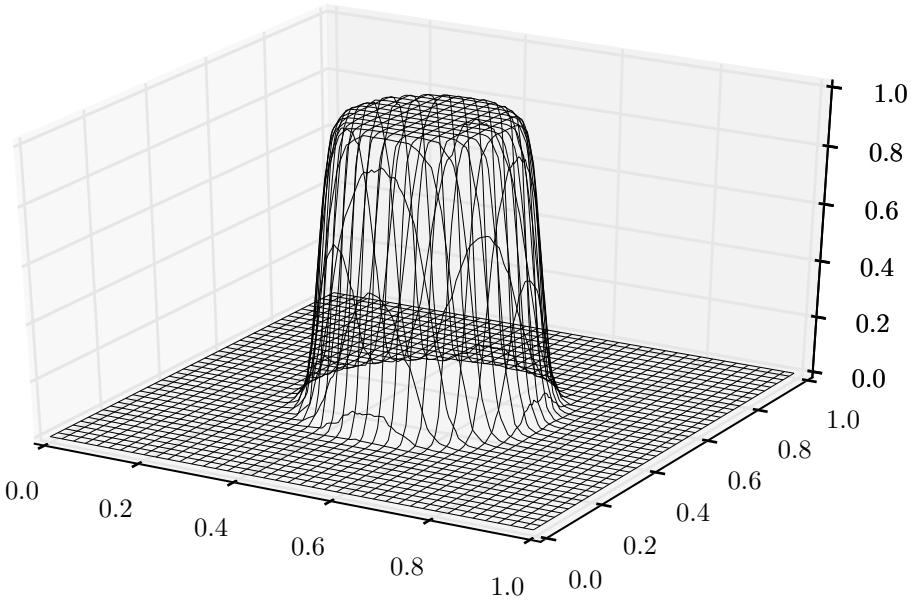

Figure 3.2: The characteristic level-set function that represents 2D bubble, i.e. circle, with the center at $(0.5, 0.5)$ and radius $r = 0.2$. Contours of this function for different levels are depicted in Fig. (3.3).

was suggested by Smereka et al. in [14] to **reinitialize** the level-set function in each time step.

Reinitialization is a simple matter of solving some advection–like equation for each physical time t. Say, we would like to reinitialize the level-set at the time t_0. We therefore solve reinitialization equation for some tentative level-set $\varphi(\mathbf{x}, \tau)$ in sub–time variable τ with the initial condition

$$\varphi(\mathbf{x}, 0) = \phi(\mathbf{x}, t_0), \ \forall \mathbf{x} \in \Omega. \tag{3.3}$$

The reinitialization is solved until steady-state, until some *steady-state criteria* is satisfied.

The original suggestion in [14] succeeds in restoration of the level-set property, but it moves the profile. Such displacement results in the loss of volume conservation.

In addition, improved reinitialization proposed by Olsson and Kreiss [15] advances in volume conservation [9]. This method considers *characteristic level-set* function ϕ_c described above and defines the reinitialization equation[2] as

$$\partial_\tau \varphi + \nabla \cdot [\varphi(1 - \varphi)\mathbf{n}_\Gamma(\mathbf{x}, t_0)] = \varepsilon \nabla \cdot [\mathbf{n}_\Gamma(\mathbf{x}, t_0)(\nabla \varphi \cdot \mathbf{n}_\Gamma(\mathbf{x}, t_0))], \tag{3.4}$$

with the inital condition (3.3), where $\mathbf{n}_\Gamma = \mathbf{n}_\Gamma(\mathbf{x}, t), \ \forall \mathbf{x} \in \Omega$ is the inner unit normal to the interface Γ pointing into the area surrounded by this interface. The parameter ε is the thickness constant, same as in the definition (3.1).

[2] It is an advection-like equation for the transport of level-set in normal vector field. Because the normal is inner, pointing into the interface, it concentrates the level set to the interface, retaining characteristic property.

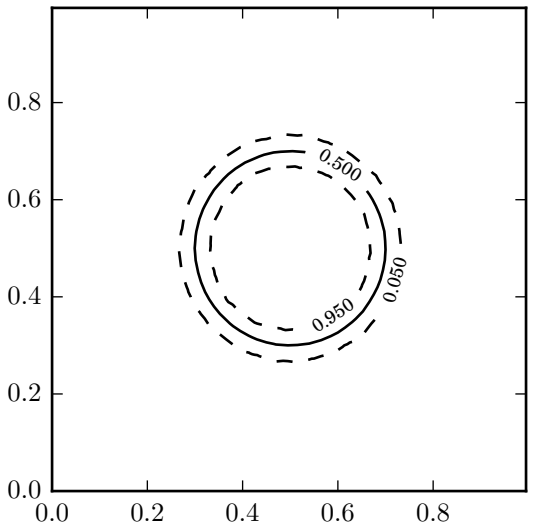

Figure 3.3: Contours of the characteristic level-set function at three different values, 0.05, 0.5 and 0.95.

In the sense of the level-set, the unit normal is given as[3]

$$\mathbf{n}_\Gamma(\mathbf{x},t) := \frac{\nabla\phi(\mathbf{x},t)}{\|\nabla\phi(\mathbf{x},t)\|}. \tag{3.5}$$

3.3 FEM for the level-set advection

As stated before, we are interested in phenomena of incompressible fluid flow. Such motion neccesarily satisfies volume conservation. Incompressibility constraint is governed by so called *divergence–free* velocity field

$$\nabla\cdot\mathbf{u} = 0,\ \forall\mathbf{x}\in\Omega.$$

Under such circumstances, transport equation (3.2) could be rewritten as

$$\partial_t\phi + \nabla\cdot(\phi\mathbf{u}) = 0. \tag{3.6}$$

Now, take $s\in\mathcal{W}_c^1$ as a test function, multiply (3.6) with s and integrate over Ω, so that weak formulation is obtained as

$$(\partial_t\phi, s) + (\nabla\cdot(\phi\mathbf{u}), s) = 0. \tag{3.7}$$

With the use of *the Gauss divergence theorem* the weak formulation yields

$$\begin{aligned}\int_\Omega s\partial_t\phi\mathrm{d}\mathbf{x} + \int_\Omega s\nabla\cdot(\phi\mathbf{u})\mathrm{d}\mathbf{x} = \\ \int_\Omega s\partial_t\phi\mathrm{d}\mathbf{x} + \int_\Omega \nabla\cdot(s\phi\mathbf{u})\mathrm{d}\mathbf{x} - \int_\Omega(\phi\mathbf{u})\cdot\nabla s\mathrm{d}\mathbf{x} = \\ \int_\Omega s\partial_t\phi\mathrm{d}\mathbf{x} + \int_{\partial\Omega} s\phi(\mathbf{u}\cdot\mathbf{n}_{\partial\Omega})\mathrm{d}S - \int_\Omega(\phi\mathbf{u})\cdot\nabla s\mathrm{d}\mathbf{x} = 0.\end{aligned}$$

[3]Note, that such normal field is defined for all $\mathbf{x}\in\Omega$, not only at the interface Γ. Also note, that in the equation (3.4), normal field $\mathbf{n}_\Gamma(\mathbf{x},t_0)$ is independent on the sub–time variable τ, so reinitialization step is solved with $\mathbf{n}_\Gamma$ constant in sub–time.

The middle term, $\int_{\partial\Omega} s\phi(\mathbf{u}\cdot\mathbf{n}_{\partial\Omega})\mathrm{d}S$ has meaning of net level-set transport into domain Ω. Assuming

$$\mathbf{u}\cdot\mathbf{n}_{\partial\Omega}\equiv 0,\ \forall\mathbf{x}\in\partial\Omega \tag{3.8}$$

the weak formulation arrives at

$$(\partial_t\phi, s) - (\phi, \mathbf{u}\cdot\nabla s) = 0. \tag{3.9}$$

The condition $\mathbf{u}\cdot\mathbf{n}_{\partial\Omega}\equiv 0,\ \forall\mathbf{x}\in\partial\Omega$ is so–called *free–slip boundary condition*, meaning the matter is free to slip on walls but must not pass through it. Otherwise, we have to take care of original weak formulation (3.7).

3.3.1 Time discretization

In the following, level-set advection is discretized in time. Say, we are seeking a solution for the advection weak formulation (3.9) $\forall t\in(0,T)$. This time interval is uniformly divided into N sub–intervals of equal length, Δt, and $t_{n+1} := t_n + \Delta t$. We also write

$$\phi^n \approx \phi(\mathbf{x}, t_n),\ \mathbf{u}^n \approx \mathbf{u}(\mathbf{x}, t_n).$$

The *Crank-Nicholson schema*[4] applied also in [9] is second order in time and states

$$\frac{1}{\Delta t}\left(\phi^{n+1}-\phi^n, s\right) = \frac{1}{2}\left(\phi^{n+1}+\phi^n, \mathbf{u}^n\cdot\nabla s\right). \tag{3.10}$$

3.4 FEM for the level-set reinitialization

With the same puprpose as in the section (3.3), take the reinitialization (3.4), multiply with $s\in\mathcal{W}_c^1$. Integrating over Ω leads

$$\int_\Omega s\partial_t\varphi\mathrm{d}\mathbf{x} + \int_\Omega s\nabla\cdot[\varphi(1-\varphi)\mathbf{n}_\Gamma]\,\mathrm{d}\mathbf{x} = \varepsilon\int_\Omega s\nabla\cdot[\mathbf{n}_\Gamma(\nabla\varphi\cdot\mathbf{n}_\Gamma)]\,\mathrm{d}\mathbf{x}. \tag{3.11}$$

Again, we rewrite the divergence terms so we can apply the Gauss theorem. It results in

$$\begin{aligned}
\int_\Omega s\partial_t\varphi\mathrm{d}\mathbf{x} + \int_\Omega \nabla\cdot[\varphi(1-\varphi)\mathbf{n}_\Gamma s]\,\mathrm{d}\mathbf{x} - \int_\Omega \varphi(1-\varphi)\mathbf{n}_\Gamma\cdot\nabla s\mathrm{d}\mathbf{x} = \\
\varepsilon\int_\Omega \nabla\cdot[\mathbf{n}_\Gamma(\nabla\varphi\cdot\mathbf{n}_\Gamma)s]\,\mathrm{d}\mathbf{x} - \varepsilon\int_\Omega(\nabla\varphi\cdot\mathbf{n}_\Gamma)\mathbf{n}_\Gamma\cdot\nabla s\mathrm{d}\mathbf{x} \Rightarrow \\
\int_\Omega s\partial_t\varphi\mathrm{d}\mathbf{x} + \int_{\partial\Omega} s\varphi(1-\varphi)(\mathbf{n}_\Gamma\cdot\mathbf{n}_{\partial\Omega})\mathrm{d}S - \int_\Omega\varphi(1-\varphi)\mathbf{n}_\Gamma\cdot\nabla s\mathrm{d}\mathbf{x} = \\
\varepsilon\int_{\partial\Omega} s(\nabla\varphi\cdot\mathbf{n}_\Gamma)(\mathbf{n}_\Gamma\cdot\mathbf{n}_{\partial\Omega})\mathrm{d}S - \varepsilon\int_\Omega(\nabla\varphi\cdot\mathbf{n}_\Gamma)\mathbf{n}_\Gamma\cdot\nabla s\mathrm{d}\mathbf{x}.
\end{aligned}$$

Repeatedly, integrals over $\partial\Omega$ vanish if level-set vanish on the boundary. With this premise we have

$$(\partial_t\varphi, s) - (\varphi(1-\varphi), \mathbf{n}_\Gamma\cdot\nabla s) = -\varepsilon(\mathbf{n}_\Gamma\cdot\nabla\varphi, \mathbf{n}_\Gamma\cdot\nabla s). \tag{3.12}$$

[4] The Crank-Nicholson schema could be viewed as a specific case of more general θ-schema with $\theta := \frac{1}{2}$ [PDE]. Simply, instead of taking "spatial" terms(terms without time derivate) fully implicit, ϕ^{n+1}, or fully explicit, ϕ^n, we take the average of both, $(\phi^{n+1}+\phi^n)/2$.

3.4.1 Time discretization

The Crank-Nicholson schema for the weak formulation (3.12) is

$$\frac{1}{\Delta\tau}(\varphi^{k+1}-\varphi^k,s)-\left(\frac{\varphi^{k+1}+\varphi^k}{2}\left[1-\frac{\varphi^{k+1}+\varphi^k}{2}\right],\mathbf{n}_\Gamma\cdot\nabla s\right)= \tag{3.13}$$

$$-\varepsilon\left(\mathbf{n}_\Gamma\cdot\nabla\frac{\varphi^{k+1}+\varphi^k}{2},\mathbf{n}_\Gamma\cdot\nabla s\right). \tag{3.14}$$

We wrote k-th time level to accentuate, that reinitialization takes place on subtime scale. This weak formulation is nonlinear(in φ).

3.5 The advection step summary

We formulated advection and reinitialization for the characteristic level-set function in the sence of weak formulation. Whole procedure could be summarized in the following

1. Initialize the level for the initial interface profile at time $t = 0$. That is, project the function (3.1) into chosen function space on the triangulation of the Ω.

2. Solve the advection equation (3.10) with given ϕ^n and $\mathbf{u}^n$ to get $\widetilde{\phi}^{n+1}$. This function is consequently reinitialized so we write $\varphi^0 := \widetilde{\phi}^{n+1}$.

3. With φ^0 from the previous step solve (3.14) until the steady state criteria leading to the level-set at the physical time t_{n+1}. Start again from step 2 to advance into next time layer.

The choice of the level-set thickness constant ε and reinitialization subtime step $\Delta\tau$ is not trivial. We use the choice from [15]

$$\begin{aligned}\Delta\tau &:= \left(\Delta x^{1+d}\right)/2,\\ \varepsilon &:= \left(\Delta x^{1-d}\right)/2,\end{aligned} \tag{3.15}$$

with the $d := 0.1$ and Δx is the spatial resolution, approximately the inverse of number of triangles in the smaller dimension, e.g. 100×100 triangles in domain has $\Delta x = 1/100$.

A domain Ω is triangulated into random-like structure of elements using *gmsh*.[5]

[5] `http://geuz.org/gmsh/`

4. The ferrofluid Navier-Stokes equations

The goal of this chapter is to formulate the equations governing ferrofluid flow, the equations of ferrohydrodynamics. In the beginning we introduce the postulates and simplifications. With the help of these we derive the dimensionless form of the Navier-Stokes equations and add force present in a magnetic field.

At the end we formulate the equations in terms of the finite element method, i.e. a weak formulation of our problem is proposed.

It is important to note, that the local-in-time existence of unique strong solution to the Cauchy problem for the system of equations of ferrohydrodynamics is given in [16]. Under the assumption that the initial data and the external magnetic field are small they also prove a global existence of strong solutions.

Let the following assumptions and simplifications hold

- ferrofluid is a *newtonian fluid*. Its stress tensor without magnetic field is

$$\mathbf{T}_n = -p\mathbf{I} + 2\eta\mathbf{D} \tag{4.1}$$

  with

$$\mathbf{D} = \frac{1}{2}\left(\nabla\mathbf{u} + (\nabla\mathbf{u})^{\mathrm{T}}\right), \tag{4.2}$$

  the rate of deformation tensor,

- ferrofluid is *linearly magnetizable, izotropic and homogenous media,* (1.4),

- there are no electric currents and ferrofluid is non-conductive medium, we work in the field of *magnetostatics*,

- the only effect of magnetic field on a ferrofluid is additional *magnetic stress tensor* $\mathbf{T}_m$ (1.11). The final stress tensor is

$$\mathbf{T} := \mathbf{T}_n + \mathbf{T}_m = -\left(p + p_s + p_m + \frac{1}{2}\mu_0 H^2\right)\mathbf{I} + 2\eta\mathbf{D} + \mu\mathbf{H}\otimes\mathbf{H}, \tag{4.3}$$

- additionaly, the ferrofluid is *incompressible*, so $\nabla\cdot\mathbf{u} = 0$. By the means of incompressibility, magneto-strictive pressure $p_s \equiv 0,\ \forall\mathbf{x}\in\Omega$.

4.1 The equations and continuous surface force approach

Let Ω be a domain. The ferrofluid domain $\Omega_1 \subset \Omega$ and $\Omega_2 := \Omega\backslash\overline{\Omega_1}$ the second phase domain.

The incompressible Navier-Stokes equations for a ferrofluid motion are

$$\boxed{\begin{aligned} \frac{\mathrm{D}(\rho\mathbf{u})}{\mathrm{D}t} &= \nabla\cdot\mathbf{T} + \mathbf{f}_s + \mathbf{f}_g, \qquad (4.4)\\ \nabla\cdot\mathbf{u} &= 0, \qquad (4.5) \end{aligned}}$$

with appriopriate boundary and initial conditions.[1] In the equation, $\rho = \rho(\mathbf{x}, t), \mathbf{u} = \mathbf{u}(\mathbf{x}, t)$ and $\frac{\mathrm{D}(\rho\mathbf{u})}{\mathrm{D}t} := \frac{\partial(\rho\mathbf{u})}{\partial t} + \mathbf{u}\cdot\nabla(\rho\mathbf{u})$ is the material derivative. The gravitational body force

$$\mathbf{f}_g = g\mathbf{e}_g \tag{4.6}$$

and the surface tension interfacial force

$$\mathbf{f}_s = \sigma\kappa\delta^*(\mathbf{x}_\Gamma)\mathbf{n}_\Gamma, \tag{4.7}$$

where σ is the surface tension coefficient measured in $\mathrm{N\,m^{-1}}$, $\kappa = \kappa(\mathbf{x}, t)$ is the curvature of the interface, $\mathbf{n}_\Gamma(\mathbf{x}, t)$ unit normal to the interface Γ and $\delta^*(\mathbf{x}_\Gamma)$ is an approximation of Dirac delta distribution "settled" at the interface Γ.

The equations formulated in (4.4, 4.5) refer to physical quantities ρ, η and μ as continuous functions of space variable $\mathbf{x}$. In contrast, it is the very nature of an interface between two different immisible fluid phases, that discontinuity in these quantities occur(at macroscopic level). To address this, discontinuities are smoothed with the help of the characteristic level set ϕ_c

$$\boxed{\begin{aligned} \rho(\mathbf{x}, t) &:= \rho_2 + (\rho_1 - \rho_2)\phi_c(\mathbf{x}, t), \qquad (4.8)\\ \eta(\mathbf{x}, t) &:= \eta_2 + (\eta_1 - \eta_2)\phi_c(\mathbf{x}, t), \qquad (4.9)\\ \mu(\mathbf{x}, t) &:= \mu_2 + (\mu_1 - \mu_2)\phi_c(\mathbf{x}, t). \qquad (4.10) \end{aligned}}$$

We can clearly see the advantage of characteristic level set over distance level set. Characteristic level set serves directly to regularize discontinuities. In case of distance level set one must construct new smoothed function and therefore introduces unasked inaccuracies.

We also adopt the notation $\rho = \rho(\phi_c(\mathbf{x}, t))$, meaning that the density, viscosity, etc. are given by level-set as in (4.8).

Now, we focus on formulation of the surface tension force and the magnetic force, both interfacial forces, in the sense of continuous surface force approach.

4.1.1 The continuous surface tension force

With the help of the level-set function ϕ_c, the approximation of Dirac delta is

$$\delta^* = \|\nabla\phi_c\|. \tag{4.11}$$

Taking unit normal as defined in (3.5) and substituting into (4.7) yields for surface tension force

$$\mathbf{f}_s = \sigma\kappa\nabla\phi_c. \tag{4.12}$$

[1] We do not specify them here, because they differ from experiment to experiment.

Comprehensive derivation of the expression (4.7) is found in [17]. The technique, where discrete surface tension force is approximated with some smoothed alternative is called *continuous surface tension (CST)* model. There is a plenty of mathematical papers with thoughtful interest in CST, its accuracy and convergence.

There is still pending some discussion about the curvature κ. In the standart level-set literature, the curvature is defined as $\kappa(\mathbf{x}) = -\nabla \cdot \mathbf{n}_\Gamma$. Instead, if we write the surface tension force as a divergence of some tensor, finite element formulation encourages us to "per-partes" the divergence onto a test function. This tensor is [18]

$$\boxed{\begin{aligned} \mathbf{T}_s &= \sigma(\mathbf{I} - \mathbf{n}_\Gamma \otimes \mathbf{n}_\Gamma)\delta^*, \\ \mathbf{f}_s &= \nabla \cdot \mathbf{T}_s, \end{aligned}} \tag{4.13}$$

$$\tag{4.14}$$

where δ^* is computed from (4.11). Advantage of this surface tension representation is the absence of curvature computation.

4.1.2 The continuous magnetic force

It was discussed in the section 1.2.4, that for linearly magnetizable ferrofluid with the absolute permeability $\widetilde{\mu} = \widetilde{\mu}(\mathbf{x}, t)$ constant within each phase separately, i.e. piecewise constant function, the magnetic force reduces to

$$\boxed{\mathbf{f}_m = -\frac{1}{2} H^2 \nabla \widetilde{\mu}.} \tag{4.15}$$

Since $\mu = \mu(\phi_c(\mathbf{x}, t))$, defined in (4.10) is an approximation of such piecewise constant permeability $\widetilde{\mu}$, we use the expression (4.15) with $\mu(\phi_c)$. The same spirit is applied in [23].

4.2 Dimensionless form

Take the Navier-Stokes equation from (4.4) and substitute gravitational force from (4.6), surface tension from (4.14), magnetic force from (4.15) and physical quantities density, viscosity and magnetic permeability from (4.8, 4.9, 4.10).

We get

$$\partial_t(\rho(\phi_c)\mathbf{u}) + \mathbf{u} \cdot \nabla(\rho(\phi_c)\mathbf{u}) = -\nabla p + \nabla \cdot (2\eta(\phi_c)\mathbf{D}) - \frac{1}{2} H^2 \nabla \mu(\phi_c) + \nabla \cdot \mathbf{T}_s + g\mathbf{e}_g. \tag{4.16}$$

Let introduce dimensionless variables

$$\mathbf{x}^* := \frac{\mathbf{x}}{x_0},\ \mathbf{u}^* := \frac{\mathbf{u}}{u_0},\ t^* := \frac{t}{x_0/u_0},\ \rho^* := \frac{\rho}{\rho_0},\ \eta^* := \frac{\eta}{\eta_0},\ \mu^* := \frac{\mu}{\mu_0},\ H^* := \frac{H}{H_0}.$$

The derivatives ∂_t and ∇ must be also non-dimensionalized. Note that after few simple arrangements, left-hand side of the equation (4.16) has dimension $\frac{u_0^2 \rho_0}{x_0}$, so we divide whole expression with this factor. Because the exact dimensional

value of the thermodynamic pressure p is not in our interest, we write p^* to note it is dimensionless and multiplied with some factor. This yields

$$\begin{aligned}\partial_{t^*}(\rho^*\mathbf{u}^*) + \mathbf{u}^*\cdot\nabla^*(\rho^*\mathbf{u}^*) = -\nabla^* p^* + \frac{1}{\mathrm{Re}}\nabla^*\cdot(2\eta^*\mathbf{D}^*)\\ -\frac{1}{\mathrm{Mg}}\frac{1}{2}(H^*)^2\nabla^*\mu^* + \frac{1}{\mathrm{We}}\nabla^*\cdot\mathbf{T}_s^* + \frac{1}{\mathrm{Fr}^2}\mathbf{e}_g,\end{aligned} \tag{4.17}$$

with the Reynolds number $\mathrm{Re} := \frac{\rho_0 u_0 x_0}{\eta_0}$ as the ratio of intertial forces to viscous forces, the Weber number $\mathrm{We} := \frac{\rho_0 u_0^2 x_0}{\sigma}$ as the ratio of inertial forces to surface tension forces, the Froude number $\mathrm{Fr} := \frac{u_0}{\sqrt{x_0 g}}$ representing the importance of inertial forces over gravitational, and the Magnetic number $\mathrm{Mg} := \frac{u_0^2\rho_0}{\mu_0 H_0^2}$ as the ratio of inertial forces to the magnetic field forces.

In the following, we omit the asterisk for brevity and work always with dimensionless quantities.

4.3 Numerical solution and projection methods

A difficulty for the numerical simulation of the incompressible Navier-Stokes equations is, that the velocity and pressure are coupled by incompressibility constraint. To overcome this difficulty, Chorin and Temam [19] proposed in the late 1960s idea of so called *projection methods*. The advantage of projection methods is that at each time one only needs to solve a sequence of decoupled elliptic equations for the velocity and the pressure. It is not our goal, to analyze the projection methods, because it is far beyond the scope of bachelor thesis. We refer more advanced reader to original paper and for overview of projection methods for incompressible flows to [20].

In this work, projection method similar to [15] is used[2].

As said, process of solution reduces to solving sequence of decoupled equations. First, we discretize the Navier-Stokes equation in time only. Spatial discretization with the help of FEM is given in the following section.

The first step is to find a *tentative velocity* $\mathbf{u}_*^{n+1}$ that does not satisfies (4.5) but $\mathbf{u}_*^{n+1} \equiv 0,\ \forall \mathbf{x} \in \partial\Omega$. That is

$$\begin{aligned}\frac{1}{\Delta t}\left(\rho^{n+1}\mathbf{u}_*^{n+1} - \rho^n\mathbf{u}^n\right) + \nabla\cdot\left(\rho^{n+1}\mathbf{u}^n\otimes\mathbf{u}_*^{n+1}\right) = -\nabla p^n\\ +\frac{1}{\mathrm{Re}}\nabla\cdot\left(\eta^{n+1}\left(\nabla\mathbf{u}_*^{n+1} + (\nabla\mathbf{u}^n)^{\mathrm{T}}\right)\right)\\ -\frac{1}{\mathrm{Mg}}\frac{1}{2}(H^{n+1})^2\nabla\mu^{n+1} + \frac{1}{\mathrm{We}}\nabla\cdot\mathbf{T}_s^{n+1} + \frac{\rho^{n+1}}{\mathrm{Fr}^2}\mathbf{e}_g.\end{aligned} \tag{4.18}$$

The second step is to solve Poisson equation for the unknown pressure p^{n+1} with $\mathbf{u}_*^{n+1}$ from the first step. This is also called *pressure correction*

$$\frac{1}{\Delta t}\nabla\cdot\mathbf{u}_*^{n+1} = \nabla\cdot\left[\frac{\nabla(p^{n+1}-p^n)}{\rho^{n+1}}\right]. \tag{4.19}$$

[2] In [15] there is no magnetic term, so addition of this term is new aspect of this thesis.

Finally, the *velocity correction* is the matter of solving

$$\mathbf{u}^{n+1} = \mathbf{u}_*^{n+1} - \frac{\Delta t}{\rho^{n+1}} \nabla (p^{n+1} - p^n). \tag{4.20}$$

We used $\rho^{n+1} = \rho(\phi_c^{n+1})$ to denote density, viscosity, etc. at $(n+1)$-th time level given by corresponding level-set.

Important note on the magnetic force term is, that it is not a function of velocity $\mathbf{u}$. Therefore, from mathematical point of view, it plays a role similar to the surface tension force and belongs to the "group forces (surface tension, gravity)" which do not change a type of equation. The only difficulty that comes with this force is the magnitude of magnetic field H^{n+1}. This value is not trivial and must be computed separately for each time step. We present whole section [eqshape] to meet this.

4.3.1 Finite element formulation

Let $\mathbf{v} \in \mathcal{W}_{vc}^2$ be a vector test function and write the $L^2(\Omega)$ inner product of $\mathbf{v}$ and the equation (4.18). We would like to "per-partes" spatial derivatives onto test function so the similar technique as in section 3.4 is adopted.

$$\begin{aligned}
\frac{1}{\Delta t} \int_\Omega \left(\rho^{n+1} \mathbf{u}_*^{n+1} - \rho^n \mathbf{u}^n \right) \cdot \mathbf{v} \mathrm{d}\mathbf{x} + \int_{\partial\Omega} \rho^{n+1} (\mathbf{u}^n \cdot \mathbf{n}_{\partial\Omega})(\mathbf{u}_*^{n+1} \cdot \mathbf{v}) \mathrm{d}S \\
- \int_\Omega (\mathbf{u}^n \cdot \nabla \mathbf{v}) \cdot (\rho^{n+1} \mathbf{u}_*^{n+1}) \mathrm{d}\mathbf{x} = - \int_{\partial\Omega} (p^n \mathbf{v}) \cdot \mathbf{n}_{\partial\Omega} \mathrm{d}S + \int_\Omega p^n \nabla \cdot \mathbf{v} \mathrm{d}\mathbf{x} \\
+ \frac{1}{\mathrm{Re}} \int_{\partial\Omega} \eta^{n+1} \left(\nabla \mathbf{u}_*^{n+1} + (\nabla \mathbf{u}^n)^{\mathrm{T}} \right) \cdot \mathbf{n}_{\partial\Omega} \mathrm{d}S \\
- \frac{1}{\mathrm{Re}} \int_\Omega \eta^{n+1} \left(\nabla \mathbf{u}_*^{n+1} + (\nabla \mathbf{u}^n)^{\mathrm{T}} \right) : \nabla \mathbf{v} \mathrm{d}\mathbf{x} \\
+ \int_\Omega \left(\frac{1}{\mathrm{Mg}} \frac{1}{2} (H^{n+1})^2 \nabla \mu^{n+1} + \frac{1}{\mathrm{We}} \int_\Omega (\nabla \cdot \mathbf{T}_s^{n+1}) + \frac{1}{\mathrm{Fr}^2} \int_\Omega \rho^{n+1} \mathbf{e}_g \right) \cdot \mathbf{v} \mathrm{d}\mathbf{x}.
\end{aligned} \tag{4.21}$$

Because we seek $\mathbf{u}_*^{n+1} \equiv 0, \ \forall \mathbf{x} \in \partial\Omega$, previous equation finally leads to FEM formulation for the first projection step omitting integrals over $\partial\Omega$.

The second, pressure correction step, is the scalar equation and pressure is approximated within space $\mathcal{W}_c^1$, so we take $q \in \mathcal{W}_c^1$, multiply and integrate over Ω,

$$\frac{1}{\Delta t} \int_\Omega q \nabla \cdot \mathbf{u}^{n+1} \mathrm{d}\mathbf{x} = \int_{\partial\Omega} q \left[\frac{\nabla (p^{n+1} - p^n)}{\rho^{n+1}} \right] \cdot \mathbf{n}_{\partial\Omega} \mathrm{d}S - \int_\Omega \left[\frac{\nabla (p^{n+1} - p^n)}{\rho^{n+1}} \right] \cdot \nabla q \mathrm{d}\mathbf{x}, \tag{4.22}$$

and similarly for the velocity correction with $\mathbf{v} \in \mathcal{W}_{vc}^2$

$$\int_\Omega \mathbf{u}^{n+1} \cdot \mathbf{v} \mathrm{d}\mathbf{x} = \int_\Omega \mathbf{u}_*^{n+1} \cdot \mathbf{v} \mathrm{d}\mathbf{x} - \Delta t \int_\Omega \left[\frac{\nabla (p^{n+1} - p^n)}{\rho^{n+1}} \right] \cdot \mathbf{v} \mathrm{d}\mathbf{x}. \tag{4.23}$$

In the equation (4.22), the boundary term is zero, if corrected pressure p^{n+1} is sought to fulfil $\nabla (p^{n+1} - p^n) \cdot \mathbf{n}_{\partial\Omega} \equiv 0, \ \forall \mathbf{x} \in \partial\Omega$. This is the unphysical boundary condition discussed in [15, 20]. It originates from the projection method and must be enforced although it can reduce the accuracy.

5. Equilibrium ferrofluid droplet shape

Complex method for a numerical simulation of ferrofluid flow is described. We would like to utilize it for prediction and simulation of equillibrium ferrofluid droplet shape.

With the *equilibrium* we refer to a state, where all forces are in balance and there is no fluid flow, so $\mathbf{u} = 0$. However, such state is hard to achieve within numerical approximation.

5.1 Problem definition

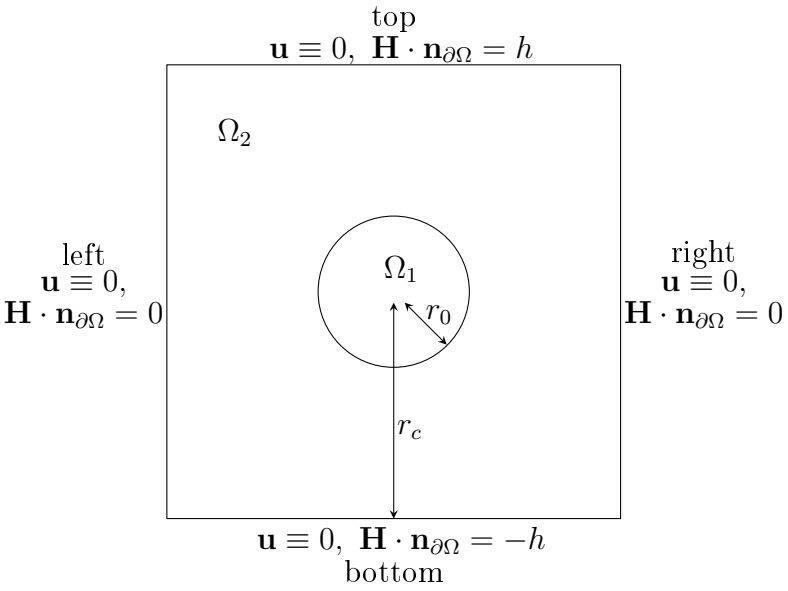

Figure 5.1: Geometry, initial and boundary condition for equilibrium droplet shape.

We have a geometry as depicted in (5.1). A ferrofluid phase Ω_1 and surrounding fluid Ω_2. The initial shape of ferrofluid droplet is circle centered at $r_c = 0.5$ with the radius $r_0 = 1/6$ so the droplet diameter takes one third of computational domain. Homogenous magnetic field of intensity g is imposed from bottom to top, i.e. in vertical direction.

Because we are interested in the equilibrium state, i.e. $\mathbf{u} = 0$, we set the viscosity of the ferrofluid equal to the viscosity of the surrounding fluid and large enough to supress time consuming droplet oscillations. We set $\eta_1 = \eta_2 = 1$ with referential $\eta_0 = 0.1$ Pa s. Surface tension is set to match surface tension of water, $\sigma = 72$ mN m^{-1}. Densities are $\rho_1 = 1, \rho_2 = 0.001$ and $\rho_0 = 1000$ kg/m^3. Dimensional referential length scale is $x_0 = 1$ cm. Surrounding fluid is assumed to be non-magnetizable, so its permeability is set to μ_0, the permeability of free space. Susceptibility of the ferrofluid phase is $\chi = 1$.

The gravity is zero in this model.

The dimensionless numbers are $\mathrm{Re} \approx 30,\ \mathrm{We} \approx 13,\ \mathrm{Mg} \approx 8$.

Domain Ω was triangulated into approximately 100×100 triangles. Dimensionless time step is set to $\Delta t = 0.005$ and spatial resolution to $\Delta x = 0.02$.

A problem remains to compute magnetic field magnitude H. It is expected, from experiments in [1] and few devoted papers [21, 22, 23], that magnetic field differs on the fluid interface. Because the magnetic force (4.15) is proportional to H^2, this difference results in non-homogenous intefrace force distribution. Magnetic force acts in the direction of applied magnetic field and elongates a droplet so it reaches ellipsoid-like shape. Ellipsoid shape with conical ends is acquired where magnetic susceptibility is large enough [24].

5.2 FEM for magnetostatics

A quest to obtain magnetic field in domain Ω and especially on the interface Γ is necessarily connected with solution of the equations of magnetostatics.

We recap them,

$$\nabla \cdot \mathbf{B} = 0,\ \nabla \times \mathbf{H} = 0,\ \mathbf{B} = \mu \mathbf{H}.$$

It should be noted, that magnetic fields simulated in this thesis are low enough, so the ferrofluid is linearly magnetizable. Roughly, according to [21], this is valid for $H < 6\ \mathrm{kA\,m^{-1}}$.

Boundary conditions imposed on the boundaries and interfaces - *the normal component* of $\mathbf{B}$ and *the tangential component* of $\mathbf{H}$ are required to be continuous. These conditions are simply derived from equations of magnetostatics and general Stokes theorem.

The ferrofluid interface Γ is represented with level-set, so boundary conditions on this interface are naturally fulfilled, because level-set represents the jump in permeabilities. Well-known magnetic scalar approach should be used, because there are no currents in ferrofluid and Ω is simply connected domain. Poisson equation is therefore solved, but simple adjustment derived in [22] helps to reduce approximation errors that originates from level-set non-zero thickness .

Boundary conditions on the interface are hence naturally fulfilled by solving the equation for an unknown magnetic scalar potential-like function $\xi = \xi(\mathbf{x}, t) : \Omega \times \mathbb{R}^+ \mapsto \mathbb{R}$,

$$\Delta \xi + \mu(\phi_c) \left(\frac{1}{\mu_2} - \frac{1}{\mu_1} \right) \delta^*(\mathbf{x}_\Gamma)(-\mathbf{n}_\Gamma) \cdot \nabla \xi = 0. \tag{5.1}$$

Note carefully, that we changed sign before normal Γ in contrast to original formulation. We have normal defined in (3.5) as inner normal.

Magnetic field induction is then obtained as

$$\mathbf{B} = \mathbf{e}_x \left(\frac{\partial \xi}{\partial y} \right) - \mathbf{e}_y \left(\frac{\partial \xi}{\partial x} \right). \tag{5.2}$$

Since we are concerned with magnetic field magnitude $H := \|\mathbf{H}\|$, using the linear constitutive relation and (5.2) we have

$$\|\mathbf{H}\| = \frac{1}{\mu(\phi_c)} \|\mathbf{B}\| = \frac{1}{\mu(\phi_c)} \sqrt{\left(\frac{\partial \xi}{\partial x} \right)^2 + \left(\frac{\partial \xi}{\partial y} \right)^2}. \tag{5.3}$$

Again, delta approximation is used as in the previous section, normal to the interafce is given as normalized level-set gradient and absolute permeability is smoothed in familiar way with the use of level-set.

Although boundary conditions on the interface Γ are naturally included in this equation, it is still required to discuss boundary $\partial\Omega$. Magnetic field $\mathbf{H}$ is applied vertical, so its normal component vanish on the right and left boundaries. This is resolved with the FEM's natural boundary conditions - Neumann's.

Weak formulation for the equation (5.1) is achieved multiplying with $r \in \mathcal{W}_c^1$, thus

$$\int_{\partial\Omega} r\nabla\xi \cdot \mathbf{n}_{\partial\Omega} \mathrm{d}S - \int_\Omega \nabla r \cdot \nabla\xi \mathrm{d}\mathbf{x} + \left(\frac{1}{\mu_2} - \frac{1}{\mu_1}\right) \int_\Omega r\mu(\phi_c)\|\nabla\phi_c\|(-\mathbf{n}_\Gamma) \cdot \nabla\xi \mathrm{d}\mathbf{x} = 0. \tag{5.4}$$

In the paper [22] finite difference method is used to solve (5.1) so implementation of (5.2) for boundary conditions is straightforward. It is now our task to solve the equation with the help of FEM.

We have noted, that first term in our weak formulation could be utilized to set boundary conditions at bottom and top. Bottom, left, top and right boundaries are denoted $(\partial\Omega)_b$, $(\partial\Omega)_l$, etc.

If we define

$$\mathbf{B}_\perp := \nabla\xi$$

we see from (5.2), that $\mathbf{B}_\perp$ is orthonormal to $\mathbf{B}$, thus $\|\mathbf{B}_\perp\| = \|\mathbf{B}\|$. This allows us to solve (5.1) with boundary conditions for our orthonormal vector field and obtain $\mathbf{B}_\perp$. The reason, why we are reformulating boundary conditions for $\mathbf{B}_\perp$ is the presence of natural Neumann's term for ξ in (5.4).

First term is rewrited into

$$\int_{\partial\Omega} r\nabla\xi \cdot \mathbf{n}_{\partial\Omega} \mathrm{d}S = \int_{(\partial\Omega)_r} r\mathbf{B}_\perp \cdot \mathbf{n}_{\partial\Omega} \mathrm{d}S + \int_{(\partial\Omega)_l} r\mathbf{B}_\perp \cdot \mathbf{n}_{\partial\Omega} \mathrm{d}S, \tag{5.5}$$

where integral over bottom and top are zero. Although original boundary conditions are $\mathbf{H}\cdot\mathbf{n}_{(\partial\Omega)_b} = -h$ and $\mathbf{H}\cdot\mathbf{n}_{(\partial\Omega)_t} = h$, orthonormal reformulation "switches" the importance to the right and left part.

Now we use the simplicity of geometry, especially $\partial\Omega$ and express the outer normal. On the $\partial\Omega$ is also $\mu = \mu_2$. Weak formulation of (5.1) is finally

$$\begin{aligned} \mu_2 \int_{(\partial\Omega)_r} rh \mathrm{d}S - \mu_2 \int_{(\partial\Omega)_l} rh \mathrm{d}S - \int_\Omega \nabla r \cdot \nabla\xi \mathrm{d}\mathbf{x} + \\ \left(\frac{1}{\mu_2} - \frac{1}{\mu_1}\right) \int_\Omega r\mu(\phi_c)\|\nabla\phi_c\|(-\mathbf{n}_\Gamma) \cdot \nabla\xi \mathrm{d}\mathbf{x} = 0. \end{aligned} \tag{5.6}$$

5.2.1 Magnetic field of ferrofluid droplet

To test the equations and method developed above, we solve a magnetic field H for some simple geometries. In figure 5.2 we can see magnetic field intensity is larger at bottom and top, comparing to the left and right sides of droplet. This demonstrates the effect responsible for the change in ferrofluid droplet shape. Magnetic force is dominant at the bottom and top and elongates the droplet.

To show the difference in magnetic force on the interface, its vector field is plotted into figure 5.3.

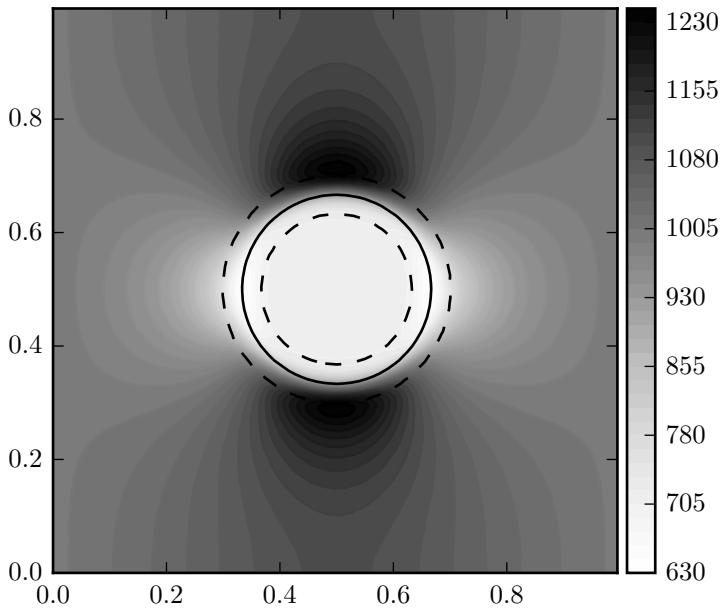

Figure 5.2: Contours of magnetic field intensity H in $\mathrm{A\,m^{-1}}$ of circular ferrofluid droplet with susceptibility $\chi = 1$ placed in non magnetic medium. Magnetic field at bottom and top is set to $h = 1\mathrm{kA\,m^{-1}}$. Contours of the level-set are drawn for values 0.05(dashed), 0.5(solid), 0.95(dashed).

5.2.2 Evolution to the equilibrium shape

Time evolution of initially circular ferrofluid droplet after imposing external magnetic field is numerically simulated. The geometry and physical parameters are defined above. The external magnetic field intensity h is varied.

Results for two different magnetic fields are shown in figures 5.4 and 5.5. The expected droplet elongation effect is apparent.

In the first subfigures, ferrofluid droplet is depicted before elongation. We can see non-structured velocity field $\mathbf{u}$ in the vicinity of the interface. That is, because the magnetic force is not yet dominant. Dominant force is surface tension force which is in the direction normal to the interface. The surface tension force is responsible for the difference in pressures, in Ω_1 and Ω_2, well known from Laplace-Young equation. This difference is within projection method slowly established through pressure correction step, so the onset of pressure is very sensitive to the time step, Δt.

Consequently, flow of fluid gets oriented and well-structured so the elongation process is initiated.

Interface changes and approaches equilibrium state. However, such state is hard to accomplish in numerical simulations. We clearly see, that although interface ceases from any further movement, velocity field $\mathbf{u} \neq 0$. There are several spurious oscilations and parasitic components, which grows fast thus we are unable to solve linear system.

Comparing equilibrium state in fig. 5.4 to fig. 5.5 simple hoped-for phe-

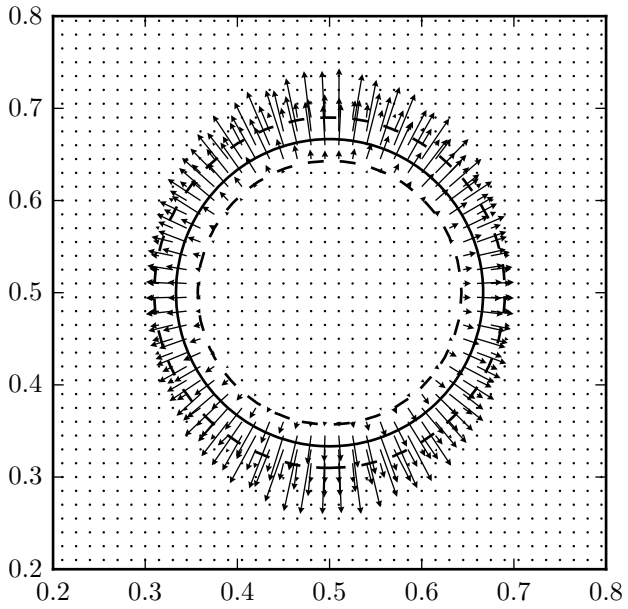

Figure 5.3: Magnetic force distribution for ferrofluid droplet with susceptibility $\chi = 1, h = 1\mathrm{kA\,m^{-1}}$. Contours of the level-set are drawn for values 0.05(dashed), 0.5(solid), 0.95(dashed). Length of vectors are scaled relatively to the figure proportions.

nomenon can be observed. The greater external magnetic field is applied, the more ferrofluid droplet elongates. This qualitative result is in accordance with [22, 24, 23].

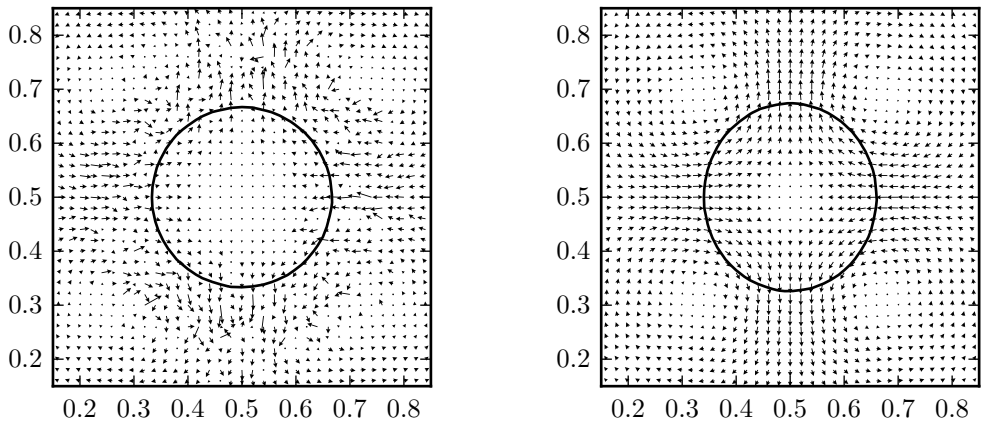

(a) $t = 0.3$ ms

(b) $t = 3$ ms

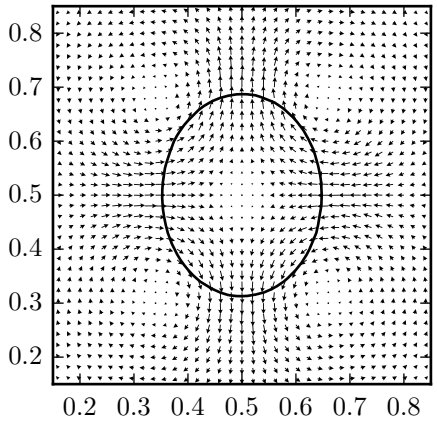

(c) $t = 6$ ms

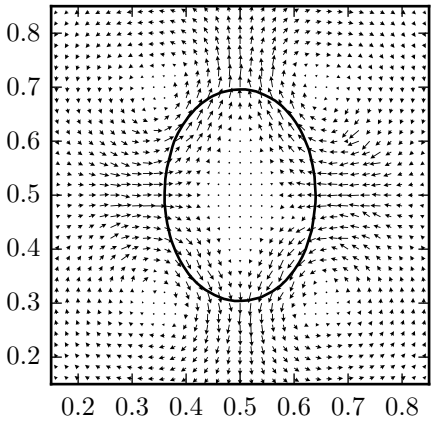

(d) $t = 9$ ms

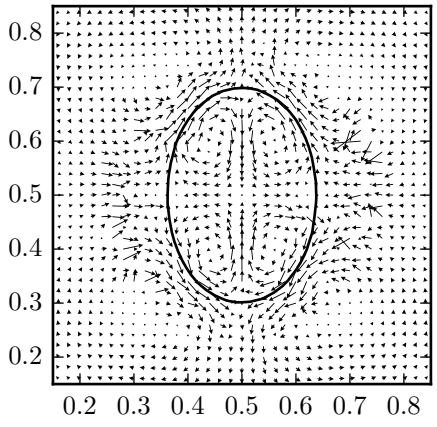

(e) $t = 12$ ms

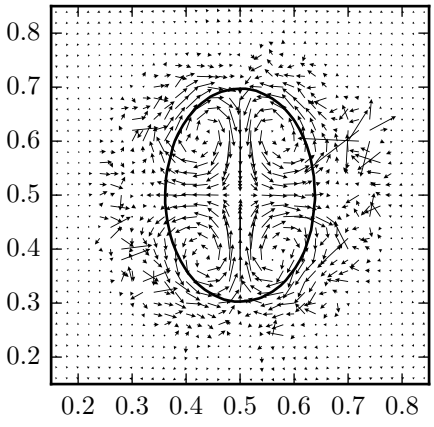

(f) $t = 15$ ms

Figure 5.4: Evolution of ferrofluid droplet in external magnetic field $h = 4\ \mathrm{kA\,m^{-1}}$. The initial diameter of droplet is 1/3 cm. Velocity field $\mathbf{u}$ is plotted, scaled relatively to the figure dimensions.

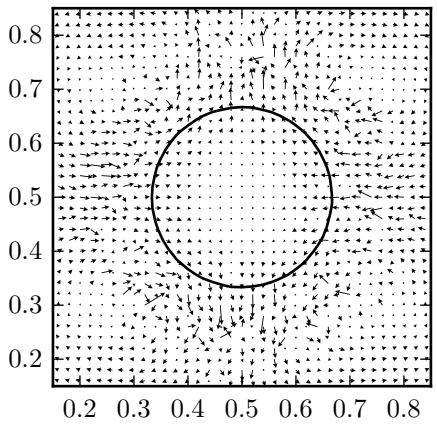

(a) $t = 0.3$ ms

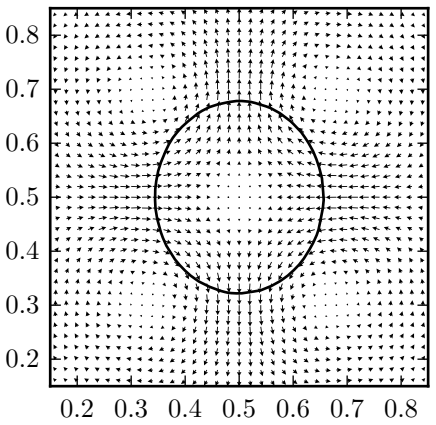

(b) $t = 3$ ms

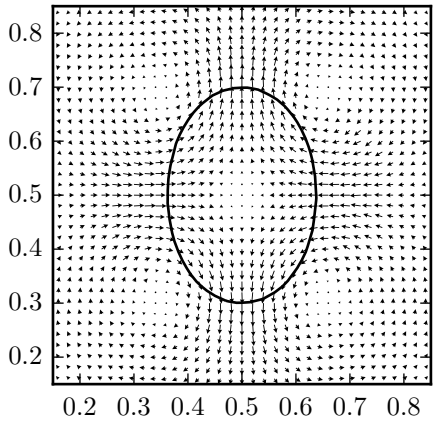

(c) $t = 6$ ms

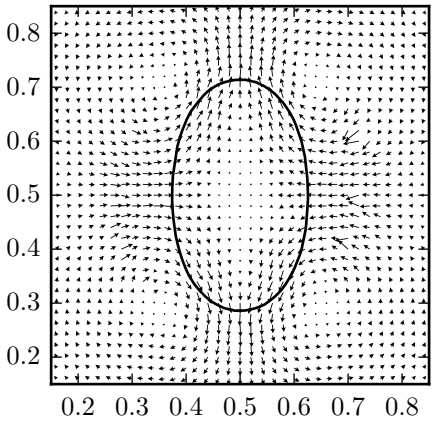

(d) $t = 9$ ms

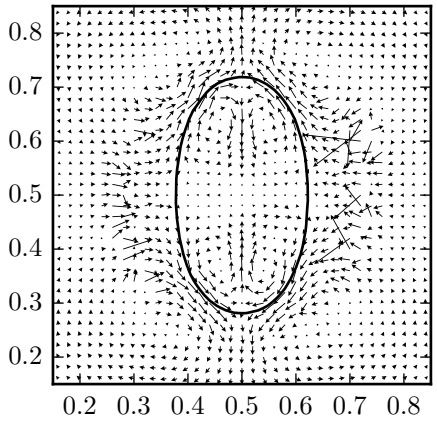

(e) $t = 12$ ms

Figure 5.5: Evolution of ferrofluid droplet in external magnetic field $h = 5\ \mathrm{kA\,m^{-1}}$. The initial diameter of droplet is 1/3 cm. Velocity field $\mathbf{u}$ is plotted, scaled relatively to the figure dimensions.

6. Ferrofluid dripping phenomenon

Equilibrium droplet shape was simulated in previous section. Because we have tested the numerical method at least in qualitative terms, it can be employed to predict the dynamics and evolution of droplet in dripping process. *Dripping* is simply a process, where droplet is hanging in the balance of surface tension and gravity force and consequently, gravity overcomes surface tension and separate droplet falls.

Since we formulated equations of motion with gravity, it is considered in the following examples.

Results given are of qualitative character. We compare observed effects with experiments in [1].

6.1 Problem definition

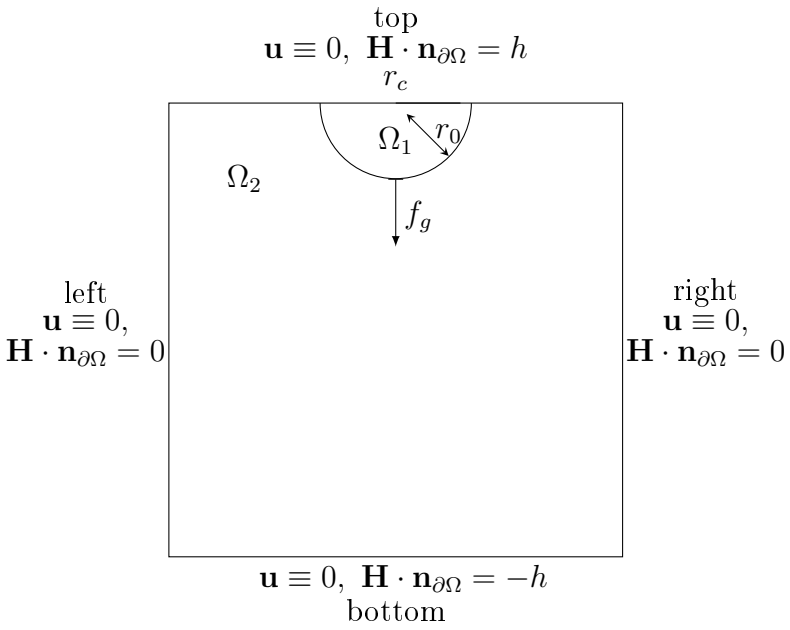

Figure 6.1: Geometry, initial and boundary condition for ferrofluid dripping phenomenon.

The geometry is depicted in (6.1). Ferrofluid initiates its motion with $\mathbf{u} = 0,\ \forall \mathbf{x} \in \Omega$ as half circle at the top boundary with diameter $r_0 = 1/6$ centered at $(0.5, 1.0)$.

It is our aim, to define the geometry and physical parameters to match the water-air simulation, so results can be compared with water-based ferrofluid experiments. Unfortunately, it is not a simple job.

Viscosities are set to $\eta_1 = 1$, $\eta_2 = 1$ and $\eta_0 = 1 \times 10^{-3}$ Pa s. Note, that actual physical viscosities of water-air model are of order 10^{-3} for water and 10^{-5} for air. Such configuration is very sensitive to spatial and time step because of high Reynolds number, and in practice tremendously computationaly costly.

Surface tension is again set to match the waters, $\sigma = 72$ mN m^{-1}. Lower surface tension would reduce spurious oscilations in the vicinity of the interface, but we found this value to be stable enough, for our spatial and time resolution. Densities are $\rho_1 = 1, \rho_2 = 0.001$ and $\rho_0 = 1000$ kg/m^3.

If we set dimensional referential length scale to x_0 similar for what we have in the equilibrium shape section, we cannot observe desired dripping phenomenon. That is simply the result of too big surface tension forces comparing to gravitational forces. From these reasons, length scale is set $x_0 = 3$ cm. Referential velocity is $u_o = \sqrt{gx_0}$.

The dimensionless numbers are $\mathrm{Re} \approx 1500,\ \mathrm{We} \approx 120, \mathrm{Fr} \approx 1,\ \mathrm{Mg} \approx 20$.

Ferrofluid phase have susceptibility $\chi = 1$ and surrounding fluid is non-magnetizable.

Domain Ω was triangulated into approximately 100×100 triangles. Dimensionless time step is set to $\Delta t = 0.005$ and spatial resolution $\Delta x = 0.015$.

6.2 Qualitative comparison

Similarly to the previous section we compute the magnetic field for initial ferrofluid droplet position. It is shown in Fig. (6.2). Such magnetic field will result in magnetic force pulling the droplet in the same direction as gravitational force. It is the effect discussed in [1].

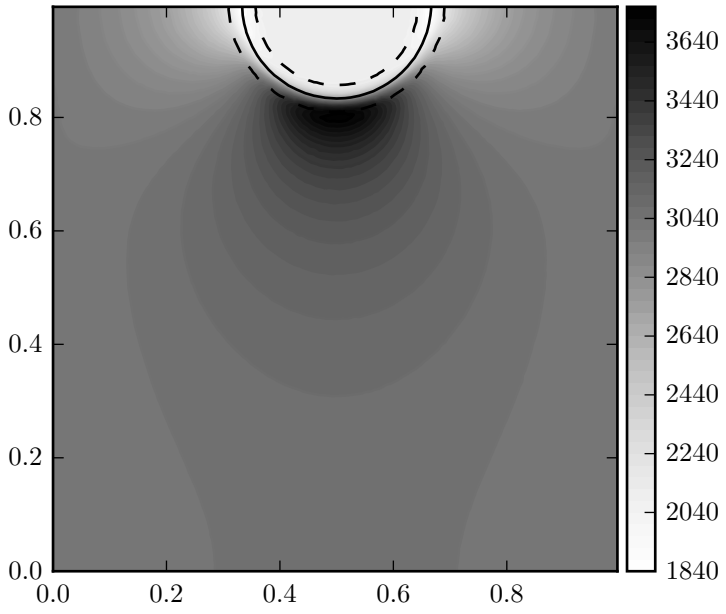

Figure 6.2: Magnetic field intensity H contours in A m^{-1} of circular ferrofluid droplet with susceptibility $\chi = 1$. Magnetic field at bottom and top is $h = 3$kA m^{-1}. Contours of the level-set are drawn for values 0.05(dashed), 0.5(solid), 0.95(dashed).

We have included the Fig. (1) to show the experimental results. Comparing to our simulations in the figures (6.3, 6.4) we can conclude, that magnetic field leads to detachment of a droplet in earlier times. In case without magnetic field, droplet is detached at time $t \approx 80$ ms whereas for magnetic field $t \approx 70$ ms.

If we have a closer look at the figures at the time of droplet separation we might note asymmetric and undulated ferrofluid interface. The origin of this inaccuracies is the low spatial resolution. So called *neck*, a very thin portion of fluid, reduces to a few triangular mesh elements and denser mesh is becoming inevitable. However, *adaptive mesh refinement* is beyond the scope of this thesis.

After the separation process neck retracts and bounces to the droplet. This is conspicuous in the last subfigures.

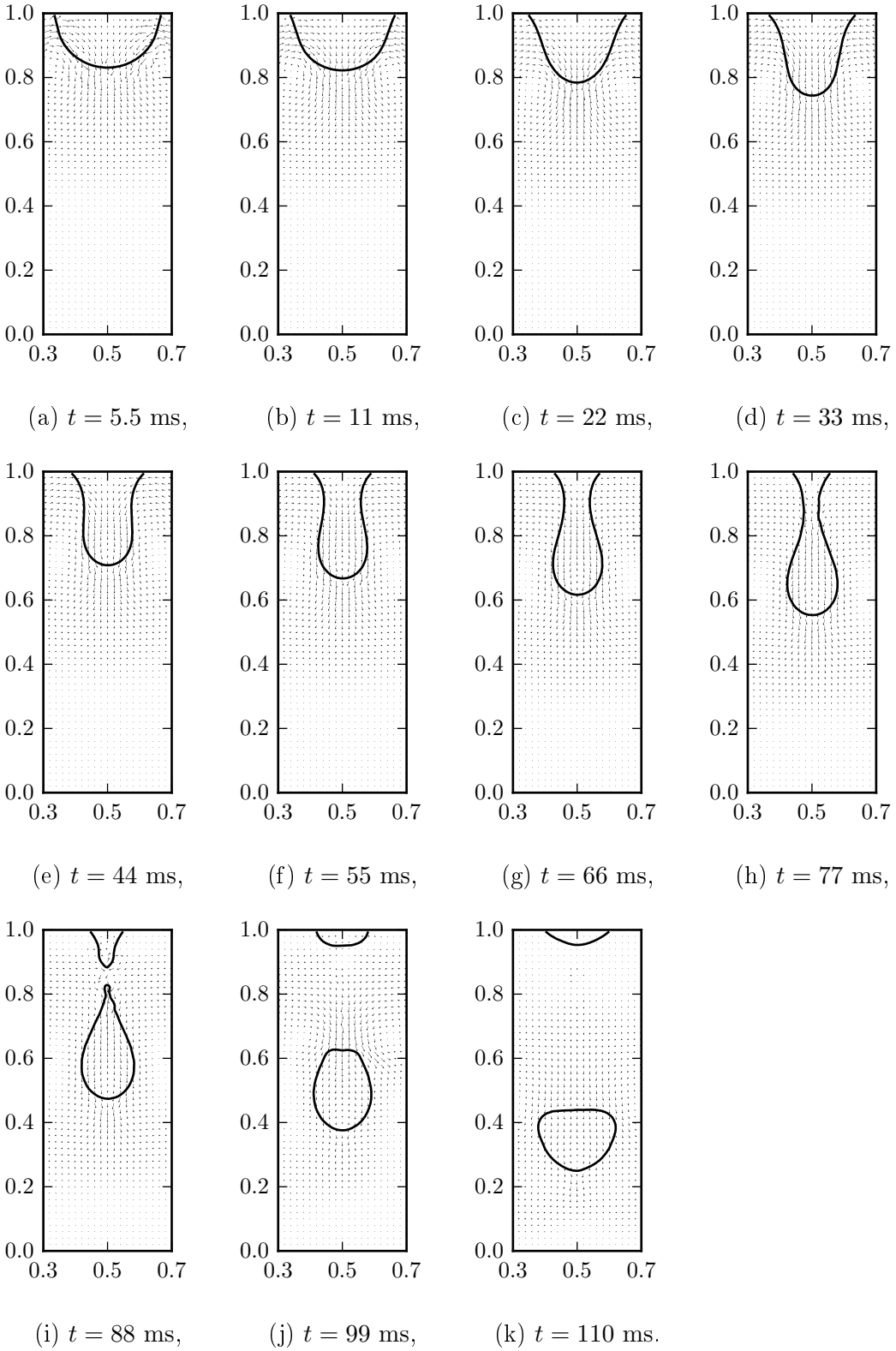

(a) $t = 5.5$ ms, (b) $t = 11$ ms, (c) $t = 22$ ms, (d) $t = 33$ ms,

(e) $t = 44$ ms, (f) $t = 55$ ms, (g) $t = 66$ ms, (h) $t = 77$ ms,

(i) $t = 88$ ms, (j) $t = 99$ ms, (k) $t = 110$ ms.

Figure 6.3: Dripping of ferrofluid droplet without external magnetic field.

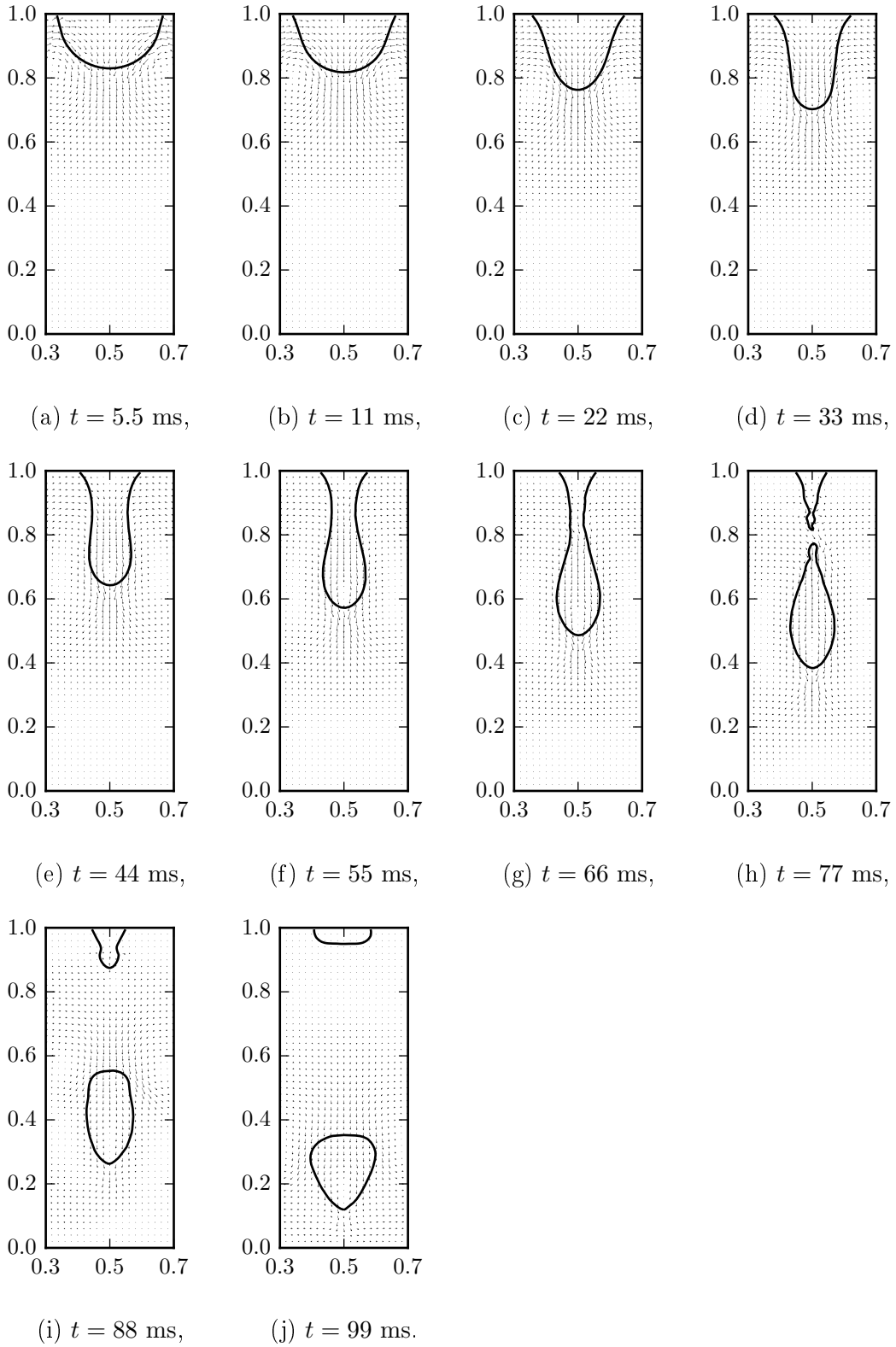

(a) $t = 5.5$ ms, (b) $t = 11$ ms, (c) $t = 22$ ms, (d) $t = 33$ ms,

(e) $t = 44$ ms, (f) $t = 55$ ms, (g) $t = 66$ ms, (h) $t = 77$ ms,

(i) $t = 88$ ms, (j) $t = 99$ ms.

Figure 6.4: Dripping of ferrofluid droplet with applied magnetic field $h = 2\ \mathrm{kA\,m^{-1}}$ at the top and bottom in the vertical direction.

Conclusion

The main goal of this thesis was to formulate the equations of ferrohydrodynamics and to put together advanced mathematical techniques, so simple free-surface ferrofluid flows can be simulated.

In the beginning, physical properties of ferrofluids are summarized and the effect of magnetic field in terms of magnetostatics is given. The influence of magnetic field is compiled into magnetic stress tensor. The magnetic force in this work acts where the permeability discontinuities are present, so this force is implemented into momentum equation as interfacial force, playing similar role to the surface tension.

In the second chapter, the heart of many modern-day numerical simulations, finite element method is briefly abstracted. Because of the complexity of the finite element method, FEniCS as the automated and efficient finite element library is used.

The third chapter is devoted to an interface tracking methods, especially to the level-set method. General mathematical formulation for characteristic level-set function is presented, together with the advection partial differential equation. Numerical deficiency of finite difference advection schemes is discussed and so called reinitialization process is included to overcome the volume of conservation inaccuracies. Advection and reinitializaion equations are discretized in time with the use of finite difference method, while weak formulation for finite element method serves for spatial discretization.

Ferrofluid Navier-Stokes equations with additional magnetic force are presented in the fourth chapter. Interfacial forces and discontinuous physical quantities are continuously approximated with the help of level-set function, i.e. continuous surface force model is adopted. The equations are non-dimensionalized, so geometry scaling becomes a simple matter of changing referential values. Velocity-pressure coupling is assured with the projection method and the final equations are spatially discretized in the sense of finite elements.

In the last chapters, necessity to solve magnetostatics Maxwell's equation is dealt with the finite element method. Some simple numerical tests are performed to validate the model and known experimental results are compared to the simulation.

We can clearly see, that applying magnetic field elongates the ferrofluid droplet because of the difference in magnetic field intensity on the droplet interface. Since interfacial magnetic force is proportional to the magnetic field intensity, droplet stretches until it is balanced with the surface tension force.

Dynamics of dripping process changes substantially. Without magnetic field, ferrofluid droplet gets slowly detached, because gravity takes a major time until droplet accelerates. In contrast, applied magnetic field stretches the droplet on relatively small time scale. Such stretched droplet is then detached earlier comparing to the case without magnetic field.

This work utilizes many numerical advancements, so solving becomes easily monstrous coupled mechanism, composed of advection, reinitialization, navier-stokes and maxwell's equations in each time step. It therefore takes a lot computational power to meet the experimental results.

The field of ferrohydrodynamics is nowadays attractive because of an outgrowth of numerical methods and progress in computational fluid dynamics. The combination of methods presented in this work is according to our best knowledge unique and not yet published.

There are also numerous possibilities to extend this work, from non-linearly magnetizable ferrofluid through implementation of asymmetric magnetic stress tensor, more accurate velocity-pressure coupling schemes to quantitative comparison with experiments.

Bibliography

[1] HABERA, Michal, Michal FABIAN, Mária ŠVIKOVÁ and Milan TIMKO. *The influence of magnetic field on free surface ferrofluid flow.* Magnetohydrodynamics. 2013, (3-4). ISSN 0024-998X.

[2] EGGERS, Jens and Emmanuel VILLERMAUX. *Physics of liquid jets.* Reports on Progress in Physics [online]. 2008, 71(3) [cit. 2015-07-29]. DOI: 10.1088/0034-4885/71/3/036601.

[3] ROSENSWEIG, Ronald E. *Ferrogidrodinamika.* Moskva: Mir, 1989, 357 s.

[4] FEYNMAN, Richard Phillips. *Feynmanovy přednášky z fyziky s řešenými příklady.* 1. vyd. Havlíčkův Brod: Fragment, 2000, 732 s. ISBN 80-7200-405-0.

[5] LANDAU, Lev Davidovič and Jevgenij Michajlovič LIFŠIC. *The classical theory of fields.* 4th rev. engl. ed. Oxford: Elsevier Butterworth-Heinemann, c1975, xiii, 428 s. Course of theoretical physics, vol. 2. ISBN 978-0-7506-2768-9.

[6] NEURINGER, Joseph L. and Ronald E. ROSENSWEIG. *Ferrohydrodynamics.* Physics of Fluids [online]. 1964, 7(12) [cit. 2015-07-29]. DOI: 10.1063/1.1711103.

[7] REDDY, J. *An introduction to the finite element method.* 2nd ed. New York: McGraw-Hill, c1993, xix, 684 s. McGraw-Hill series in mechanical engineering. ISBN 0070513554.

[8] BRENNER, Susanne C. *The mathematical theory of finite element methods.* 2nd ed. New York, NY: Springer-Verlag, 2002, xv, 361 s. ISBN 0-387-95451-1.

[9] LINDBO, Dag. *Finite Element Computations for a Conservative Level Set Method Applied to Two-Phase Stokes Flow.* Stockhom, Sweden, 2006. Available also at: `http://www.karlin.mff.cuni.cz/~hron/NMMO403/lindbo_dag_06153.pdf`. Master thesis. School of Computer Science and Communication, Stockholm, Sweden.

[10] ALNAES, M.S., A. LOGG, K A. MARDAL, O. SKAVHAUG and H.P. LANGTANGEN. *Unified framework for finite element assembly.* International Journal of Computational Science and Engineering [online]. 2009, 4(4) [cit. 2015-07-29]. DOI: 10.1504/ijcse.2009.029160.

[11] OLSSON, Elin and Gunilla KREISS. *A conservative level set method for two phase flow.* Journal of Computational Physics [online]. 2005, 210(1): 225-246 [cit. 2015-07-29]. DOI: 10.1016/j.jcp.2005.04.007.

[12] MAITRE, Emmanuel. *Review of numerical methods for free interfaces.* Les Houches, 2006. Available also at: `http://pmc.polytechnique.fr/mp/GDR/docu/Maitre.pdf`.

[13] EVANS, Lawrence C. *Partial differential equations.* 2nd ed. Providence, R.I.: American Mathematical Society, c2010, xxi, 749 p. Graduate studies in mathematics, v. 19. ISBN 0821849743.

[14] SUSSMAN, Mark, Emad FATEMI, Peter SMEREKA and Stanley OSHER. *An improved level set method for incompressible two-phase flows.* Computers & Fluids [online]. 1998, 27(5-6): 663-680 [cit. 2015-07-29]. DOI: 10.1016/s0045-7930(97)00053-4.

[15] OLSSON, Elin, Gunilla KREISS and Sara ZAHEDI. *A conservative level set method for two phase flow II.* Journal of Computational Physics [online]. 2007, 225(1): 785-807 [cit. 2015-07-29]. DOI: 10.1016/j.jcp.2006.12.027.

[16] TAN, Zhong and Yanjin WANG. *Global analysis for strong solutions to the equations of a ferrofluid flow model.* Journal of Mathematical Analysis and Applications [online]. 2010, 364(2): 424-436 [cit. 2015-07-29]. DOI: 10.1016/j.jmaa.2009.10.032.

[17] BRACKBILL, J.U, D.B KOTHE and C ZEMACH. *A continuum method for modeling surface tension.* Journal of Computational Physics [online]. 1992, 100(2): 335-354 [cit. 2015-07-29]. DOI: 10.1016/0021-9991(92)90240-y.

[18] LAFAURIE, Bruno, Carlo NARDONE, Ruben SCARDOVELLI, Stéphane ZALESKI and Gianluigi ZANETTI. *Modelling Merging and Fragmentation in Multiphase Flows with SURFER.* Journal of Computational Physics [online]. 1994, 113(1): 134-147 [cit. 2015-07-29]. DOI: 10.1006/jcph.1994.1123.

[19] CHORIN, Alexandre Joel. *Numerical solution of the Navier-Stokes equations.* Mathematics of Computation [online]. 1968, 22(104): 745-745 [cit. 2015-07-29]. DOI: 10.1090/s0025-5718-1968-0242392-2.

[20] GUERMOND, J.L., P. MINEV and Jie SHEN. *An overview of projection methods for incompressible flows.* Computer Methods in Applied Mechanics and Engineering [online]. 2006, 195(44-47): 6011-6045 [cit. 2015-07-29]. DOI: 10.1016/j.cma.2005.10.010.

[21] AFKHAMI, S., A. J. TYLER, Y. RENARDY, M. RENARDY, T. G. St. PIERRE, R. C. WOODWARD and J. S. RIFFLE. *Deformation of a hydrophobic ferrofluid droplet suspended in a viscous medium under uniform magnetic fields.* Journal of Fluid Mechanics [online]. 2010, 663: 358-384 [cit. 2015-07-29]. DOI: 10.1017/s0022112010003551.

[22] KI, Hyungson. *Level set method for two-phase incompressible flows under magnetic fields.* Computer Physics Communications [online]. 2010, 181(6): 999-1007 [cit. 2015-07-29]. DOI: 10.1016/j.cpc.2010.02.002.

[23] SHI, Dongxiao, Qincheng BI and Rongqi ZHOU. *Numerical Simulation of a Falling Ferrofluid Droplet in a Uniform Magnetic Field by the VOSET Method.* Numerical Heat Transfer, Part A: Applications [online]. 2014, 66(2): 144-164 [cit. 2015-07-29]. DOI: 10.1080/10407782.2013.869459.

[24] LAVROVA, O., V. POLEVIKOV and L. TOBISKA. *Equilibrium shapes of a ferrofluid drop.* PAMM [online]. 2005, 5(1): 837-838 [cit. 2015-07-29]. DOI: 10.1002/pamm.200510390.

List of Tables

Tab. 2.1 Finite element spaces.

List of Abbreviations

FHD ferrohydrodynamics,
EHD electrohydrodynamics,
MHD magnetohydrodynamics,
FEM finite element method,
LSM level-set method,
CST continuous surface tension.